Master's thesis

NTNU
Norwegian University of Science and Technology
Faculty of Engineering
Department of Geoscience and Petroleum

Ujjwal Shekhar

Effective Seismic model from Fractured rock

Master's thesis in Petroleum Geosciences
Supervisor: Alexey Stovas
June 2021

NTNU
Norwegian University of
Science and Technology

Ujjwal Shekhar

Effective Seismic model from Fractured rock

Master's thesis in Petroleum Geosciences
Supervisor: Alexey Stovas
June 2021

Norwegian University of Science and Technology
Faculty of Engineering
Department of Geoscience and Petroleum

NTNU
Norwegian University of
Science and Technology

Norges Teknisk-Naturvitenskapelige Universitet
Department of Geoscience and Petroleum

NTNU

TPG4925 - Petroleum Geosciences - Master's Thesis

Effective Seismic model from Fractured rock

June 15, 2021

Spring 2021:
Ujjwal Shekhar
Candidate No.10005

Supervisor: Alexey Stovas, IGP, NTNU

Effective Seismic model from Fractured rock

by

Ujjwal Shekhar

A thesis submitted in partial fulfillment of the requirements for the degree of

Master of Science

in

Petroleum Geophysics

June 2021

Faculty of Engineering,
Department of Geoscience and Petroleum

Norwegian University of Science and Technology

NTNU

Abstract

Analyses of vertical fractures are of great interest in characterizing the fluid flow and minimum in situ stress direction in reservoirs. Fractures are responsible for permeability anisotropy in a reservoir. Fractures can be the cause of migration of hydrocarbons, leakage of drilling fluid and even release of gases like methane on seabed. There is a need to extensively study the small-scale fractures, embedded in host rock to understand the challenges in exploitation of fractured reservoirs. Nowadays, technologies for carbon capture and storage (CCS) are gaining popularity. CCS involves massive injection of carbon dioxide into the subsurface, thereby altering the stress state in the reservoir. Fractures play a vital role in the mobilization of CO_2. Knowledge about fracture systems in the subsurface formation can help estimate a threshold value of volume to be injected. This may prevent leakage of gas to atmosphere in case of onshore reservoir or into the ocean water for offshore reservoir and potential seismic hazard induced by injection activities. Presence of small scale fractures can be detected in the drilled cores. However, this gives us information about fractures over a very small area only. By using seismic attributes, we get such information on a broader scale. The importance of this work may be realized by considering the cost involved in drilling a borehole. It is to be noted that tremendous amount of seismic data acquired over some of the major fractured reservoirs in the world are already available. And the expressions for numerical computation of seismic attributes using fracture parameters are straightforward and simple.

Long-wavelength equivalent orthorhombic (ORT) media and monoclinic media typically characterize the anisotropy induced by a set (or two sets orthogonal to each other) of vertical parallel fractures and two non-orthogonal sets of vertical fractures respectively, embedded into a transversely isotropic medium with a vertical symmetry axis (VTI). In nature, transverse isotropy is usually displayed by sedimentary rocks, planar igneous bodies and floating ice sheets. The equivalent stiffness matrix for the Vertically Fractured media with Transverse Isotropy (VFTI) and monoclinic media are derived from the background stiffness coefficients and fracture weaknesses parameters. The goal of this thesis work is to accurately model fractures and analyze the fracture response in normal move-out velocities (defined by traveltimes) and gradient term in the reflection coefficient of the amplitude vs azimuth attributes for different wave modes. These responses are based on changes in the orientation of fracture sets and the magnitude of fracture weaknesses. These seismic data, acquired over a fractured reservoir can also be inverted for the azimuth angles of fracture sets present in the host rock.

In the first part, study has been carried upon VFTI media. A term called eccentricity of the normal move-out (NMO) velocities ellipse is defined. We will see the sensitivities towards fracture weaknesses in the eccentricity term for pure wave modes (PP, S_1S_1, S_2S_2) and converted wave modes (PS_1, PS_2, S_1S_2). Similar study on amplitude vs azimuth (AVAz) analyses of fractured media is done. Sensitivities towards fracture weaknesses in the gradient term of reflection coefficients for pure wave modes (PP, S_VS_V, S_HS_H) and converted wave modes (PS_V, PS_H and S_VS_H) are determined.

In the second part, fracture response in NMO velocities and gradient term in the reflec-

tion coefficient of AVAz attributes for different wave modes are observed for monoclinic media. Inverse modeling study that aims to determine the orientation of fracture systems from the given seismic data has been carried out. The error in azimuth angle of fracture sets for such inversion technique has been calculated.

Finally, sensitivities towards fracture parameters established from both attributes are compared. The advantages and limitations of both data sets are then discussed. Apart from a standard model, the study has also been carried upon two arbitrary models, the VTI background medium of which are derived from upscaling of well log data. Generalized conclusions about the applicability of results so obtained have been made.

Contents

List of Figures

List of Tables

List of Symbols

ϕ	Phase azimuthal angle
θ	Phase polar angle
Θ	Group polar incident angle
Φ	Group polar azimuth angle
ρ	Density of the rock
σ_{ij}	Stress tensor
ϵ_{ij}	Strain tensor
c_{ij}	Stiffness coefficients
V_p	P-wave velocity
V_s	S-wave velocity
Γ	Tensor function of slowness vector s
$(n_1, n_2, n_3)^T$	Phase-directional vector
$\delta_N, \delta_V, \delta_H$	Fracture weaknesses
ϵ, γ, δ	Thomsen anisotropic parameters
K	Fracture compliances
ξ	Monoclinic anisotropic parameter

1 Introduction

Fractures affect the permeability of the rock. This creates directional preferences for flow of the fluid. The almost ubiquitous presence of fractures in the subsurface and their tendency to provide natural pathways for hydrocarbon flow makes them an important target in the exploration and exploitation of oil and gas reservoirs (Grechka and Kachanov, 2006). Wave propagation through fractures and faults is an important topic in seismology and exploration geophysics. Faults in the earth's crust constitute sources of earthquakes (Pyrak-Nolte et al., 1990). Applications in geotechnical engineering, such as analysis of the dynamic stability of rock slopes and tunnels, involve the study of imperfect joints in rock masses (Perino et al., 2010; Fan et al., 2011). Nowadays, geomechanical characterization of the subsurface by integrating laboratory data with well logs and seismic data to assess in-situ stresses and reservoir/cap rock integrity has become prominent. In the first section, the derivation of equivalent orthorhombic and monoclinic medium moduli, and slowness surface for a fractured medium with transversely isotropic background (VTI) is sketched. For numerical examples in the report, I used a standard model (Schoenberg and Helbig, 1997) believed to be typical of vertically fractured shale. In the next section, I analyzed the NMO (normal moveout) velocities ellipse for vertically fractured media with transverse isotropy (VFTI) and monoclinic media. Further, amplitude vs azimuth (AVAz) response in gradient terms of reflection coefficients for the two layered model, in which one of the layer is VFTI or monoclinic and the other is VTI is also studied. Later, sensitivities towards fracture weaknesses and orientation of fracture sets for both attributes are found and compared. Inverse modeling study that aims to determine the orientation of fracture sets using NMO ellipses data is carried out.

1.1 Fractured rocks and fractured reservoirs

Sedimentary rocks (for example, shale, sandstone, etc.) are naturally fractured. The natural fractures are mostly sealed by material that have precipitated in them throughout the geologic time. Natural fractures are diagenetic fractures and/or tectonic fractures. These are mechanical breaks in rocks, which form in nature, in response to lithostatic, tectonic and thermal stress, and high fluid pressure. Shale is fissile and laminated. "Laminated" means that the rock is made up of many thin layers. "Fissile" means that the rock readily splits into thin pieces along the laminations.

Some of the largest fields in the world are fractured. Examples are Haft Kel field in Iran, Sprawberry field in the United States of America, Kirkuk in Iraq and North Sea chalk fields (Ekofisk, Valhall) in the offshore Norway. A fractured reservoir is one in which naturally occurring fractures either have or are predicted to have a significant effect on reservoir fluid flow in the form of (1) increased reservoir permeability, (2) increased porosity, and/or (3) increased permeability anisotropy (AAPG wiki). A reservoir is defined as being fractured only if a continuous network of fractures is distributed throughout the reservoir. If continuous fracture network exists in a reservoir, there can be significant

[a]  [b]  [c] 

Figure 1: Fractures in sedimentary rocks: a) Set of parallel vertical fractures (Gondwana basin, Ara- Dumerbera, India). b)Vertical fracture in the cross-sectional view (Gondwana basin, Ramgarh, India). c)Non-orthogonal fracture sets (Gondwana basin, India)

mud losses during drilling . Naturally fractured reservoirs are in general more sensitive to changes in stress or geomechanical behavior when fracture aperture or permeability is strongly influenced by rock deformation in fractured rock (Bagheri and Settari, 2008).
Four basic types of reservoir fractures can be defined:
Type 1—Provide the essential porosity and permeability to the reservoir.
Type 2—Provide the essential permeability.
Type 3—Provide a permeability assist to an already producible reservoir.
Type 4—Impart no positive reservoir quality but create strong reservoir anisotropy and inhomogeneity.
Two terms that are important in context to fractured reservoirs and are frequently used in this study are fracture system and fracture network. **Fracture system** is a set of parallel fractures in host rock. **Fracture network** is two or several associated fracture systems.

1.2 Importance of fracture analysis

Naturally fractured reservoirs exist throughout the world and represent significant amounts of oil and gas reserves, water, and other natural resources on Earth. In the past half-century, the study of fluid flow and transport processes in fractured porous media has received great attention and has been one of the most active areas in investigating multi-phase flow (Yu-Shu Wu, 2016) in subsurface reservoirs. This is because of its importance to underground natural-resource recovery, waste storage and disposal, environmental remediation, CO_2 geosequestration, and many other subsurface applications. Reservoir performance is dictated by origin and distribution of natural fractures. Also, Reservoir development is impacted by natural fractures. In heterogeneous reservoirs, the dominant flow mechanism is through the network of fractures rather than the reservoir matrix. In the petroleum industry, naturally fractured reservoirs are generally characterized by dual porosity system. Barenblatt, Zheltov, and Kochina (1960) first introduced the concept of a dual porosity model, which presents two distinctive porous regions with different

properties. The dual porosity model assumes that the matrix has ample storage capacity, but low permeability compared with the natural fracture system. The fractures are assumed to have little storage capacity but high permeability relative to the matrix system.
The system of natural fractures in the area being developed is only confirmed by detecting (using logs, video, core, etc.) the presence of the intersection of these natural fractures with the wellbore. But, there are techniques (with few assumptions) to understand more about fractures, even for the whole field in general. The major information deciphered using such approach is how many fracture systems could possibly be present in the area, with their respective strike directions(trend). This work aims to identify the fracture systems based on seismic data considering an effective media theory. Here, the underlying assumptions are that the fractures are long, thin, vertical and are uniformly distributed in the rock matrix. So, fractures are the main cause of azimuth anisotropy in seismic velocities.

1.3 Objective of the study

The NMO velocities ellipse and AVAz gradient terms can be defined for different wave modes with the help of backgound stiffnesses and fracture weaknesses parameters. The goal of this work is to find the sensitivities of NMO velocities ellipse and AVAz gradient towards fracture weaknesses and orientation of the fracture sets and then compare both data set. In the case of monoclinic media, emphasis has been made on the sensitivity of NMO group velocity ellipses for P, S_1 and S_2 waves toward fractures. I carried out two type of modeling work, namely forward and inverse. In the forward modeling, information about the azimuth angle of fracture sets are known and group velocity coefficients for different wave modes are determined with the help of VTI backgound stiffnesses and fracture weaknesses values. In the inverse modeling, the orientation of fracture sets are determined from the given NMO group velocity ellipses for P, S_1 and S_2 waves. The errors in computation of azimuth angles of fracture sets are then found out and decision on choosing wave modes best suited for this inversion is made.

2 Fractured medium

Fracturing in rocks is quite common phenomenon and can be easily observed on surface. The scale of fractures may vary. If the scale of fracturing is large enough and sufficient displacement of the strata around this fracture has taken place, it is termed as fault. In most of sedimentary rocks, this small scale fractures are the cause of seismic anisotropy. Presence of such fractures alongwith their host rock forms the fractured medium.

2.1 General theory

Fractures are induced by stress. The rocks in the subsurface are under the action of triaxial stress field. This stress field generally consists of two inequal horizontal (tectonic) principal stresses and a vertical principal stress caused by the overburden weight.

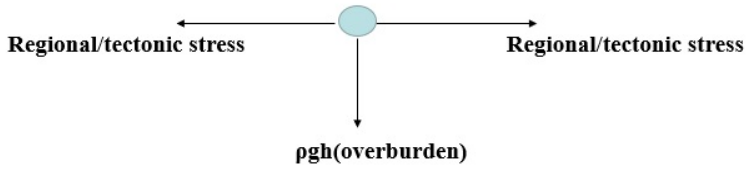

Figure 2: Triaxial nature of stress in the Earth's crust

This leads to the formation of vertical fractures in rock body. Geological fractures are pairs of distinctly separated surfaces in the formation which are related to permanent rock crack deformation (Jaeger, 1969; Priest and Hudson, 1976; Schultz and Fossen, 2008). The resulting rheology is usually effective anisotropy with orthorhombic or monoclinic symmetries.

2.2 Seismic response from fractured medium

Wave propagation velocity strongly depends on the ratio (λ/d) of the dominant wavelength to the typical layer thickness (Stovas and Arntsen, 2006). When the frequency is very low (zero frequency limit) or the wavelength is quite large compared to the layer thickness, the wave velocity can be given by an average of the properties in individual layers (Backus, 1962), and waves behave as if propagating in an effective homogeneous medium. On the other hand, when the frequency is very high (infinite frequency limit), the waves behave in line with the ray theory. In reality however, neither zero nor infinite frequency limit is reached and the acquisition of seismic data is usually carried out under band of frequencies. The intensity in response of seismic waves depends on several factors, one being nature of the fracture filling material. Generally, gas-filled (dry) fractures generate stronger responses of both reflections and diffractions than liquid-filled fractures. But the effects of filling material on seismic responses has not been discussed in this report.

2.2.1 High frequency limit

Under high frequency limit, each of the individual components of the geological structure will influence the transmitted waves according to optical ray theory. The elastic wave velocity of such a medium can be highly dispersive and scattering of wave is common. For near-vertical fractures, and also for fracture clusters, diffraction from the fracture tips is observed. It is cumbersome understanding true structural scaling within the Earth and so working with seismic data at this limit is extremely inconvenient. The response from a vertical fracture is governed by two factors, such as the angle of incidence and the degree of fracture opening (aspect ratio). When a fracture has a small opening ($AR < 1/1000$) and an energy source is located at the projection of the fracture onto the surface, the incident wave propagates vertically downward and tangentially to the fracture, thus producing almost no reflection. When a fracture has a small opening and the incident wave propagates from an energy source located away from the fracture projection onto the surface, the seismic response is recorded as diffracted compressional and diffracted converted waves with minimal arrival times at the projection point (Leviant et. al., 2019). Numerical simulation of the wave responses from near vertical fractures illustrates one more of their properties, asymmetry of the diffraction, i.e., a difference between their left and right parts, even at a small deviation from the vertical. Increasing the deviation angles enhances this difference.

2.2.2 Low frequency limit

At low frequency limit, layered structure behaves as one 'effective' medium. For most of the practical purposes, exploiting seismic data under low to moderate frequency limit is advantageous in making precise and cost saving analysis. Instead of working with numerous small scale heterogeneity, one simply deals with a homogeneous anisotropic media. This also make it suitable for inversion studies.

Two popular effective media theories have been proposed by Hudson (1980) and Schoenberg (1980). These theories originally were developed for a single set of rotationally invariant cracks embedded in isotropic host rock and later were extended to several fracture sets and to anisotropic backgrounds (Schoenberg and Helbig, 1997).
Linear slip theory: According to the linear slip theory , the small vector difference across a fracture, in the displacement, is assumed to depend linearly on the traction vector (Jones and Whittier, 1967; Schoenberg, 1980). With the low frequency limit assumption, a linear slip interface is equivalent to a fracture interface that satisfies the nonwelded contact boundary conditions. Therefore, the fractured medium can be regarded as a combination of a fracture, or a set of fractures, and a background or host medium.
The theory on models of cracks (Kachanov, 1980) predicts that the symmetry of effective anisotropy induced by dry cracks is close to orthorhombic regardless of the number of fracture sets, their crack densities, and their orientations.

Backus averaging

A transversely isotropic, stratified medium is considered, whose axis of symmetry is vertical and whose properties vary only in vertical direction and not in horizontal plane. The medium may be locally isotropic. A length l' is chosen arbitrarily. The results which follow are true for any l', but are useful only if l' is large enough so that the properties of the medium are significantly smoothed by averaging over a vertical distance l'. The response of the medium to elastic waves whose wave numbers k are much less than $2\pi/l'$ can be calculated. The medium is replaced by a 'long-wave equivalent' (Backus, 1962) transversely isotropic medium, whose density is the average density (averaged locally over a vertical length l', and whose five elastic parameters are calculated from the parameters of the original medium by means of arithmetric averaging operators:

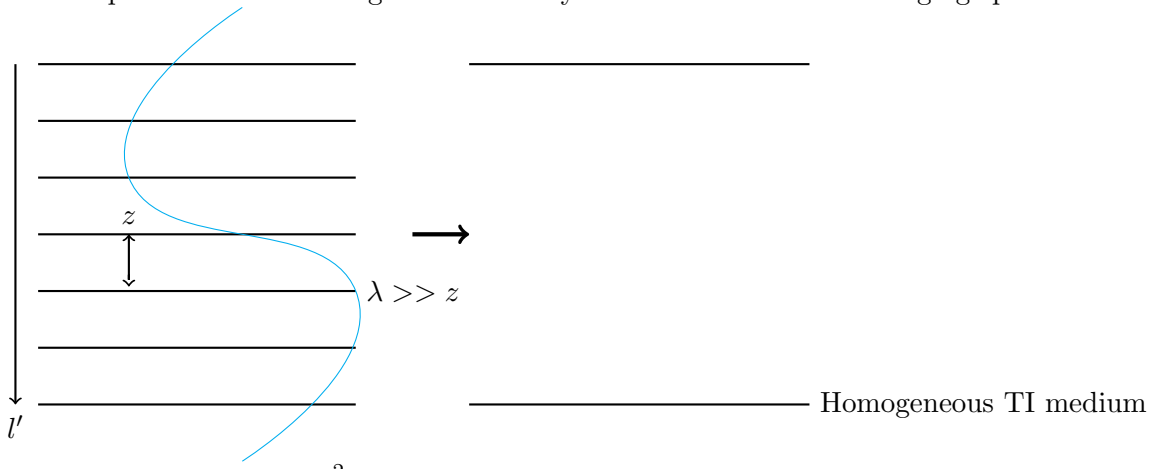

$$c_{11e} = \left\langle c_{11} - \frac{c_{13}^2}{c_{33}} \right\rangle + \left\langle \frac{c_{13}}{c_{33}} \right\rangle^2 \left\langle c_{33}^{-1} \right\rangle^{-1}$$
$$c_{13e} = \left\langle \frac{c_{13}}{c_{33}} \right\rangle \left\langle c_{33}^{-1} \right\rangle^{-1}$$
$$c_{33e} = \left\langle c_{33}^{-1} \right\rangle^{-1}$$
$$c_{44e} = \left\langle c_{44}^{-1} \right\rangle^{-1}$$
$$c_{66e} = \langle c_{66} \rangle$$
$$\rho_e = \langle \rho \rangle$$

where, the effective system matrix M_e is given by a simple arithmetric mean of all system matrices M_j from the stack of N equally spaced layers. The thickness of each layer is **z**.

$$M_e = \langle M \rangle = \frac{1}{N} \sum_{j=1}^{N} M_j$$

2.3 Fracture induced seismic anisotropy

Seismic anisotropy is defined as the dependence of seismic velocity upon angle. Anisotropy should not be confused with heterogeneity. Heterogeneity is the dependence of physical properties upon position. Heterogeneity on the small scale can appear as seismic anisotropy on the large scale. Seismic velocity anisotropy can be caused by different factors, such as rock fabric, grain-scale microcracks, rock layering and aligned fractures at all scales, provided that the characteristic dimensions of these features are small relative to the seismic wavelength (Worthington, 2008). Fracturing of rock can induce lower symmetry seismic anisotropy. A medium with vertical fractures can be effectively described in terms of an anisotropic model with orthorhombic (ORT) or monoclinic symmetry (Schoenberg and Sayers, 1995).

2.3.1 HTI anisotropic model

The transversely isotropic model with a horizontal symmetry axis (HTI) has two mutually orthogonal vertical planes of symmetry (Tsvankin, 1997). The Regional stress is a dominant factor in this case. A system of one set of parallel vertical fractures in an isotropic rock matrix could result in HTI type of anisotropy model.

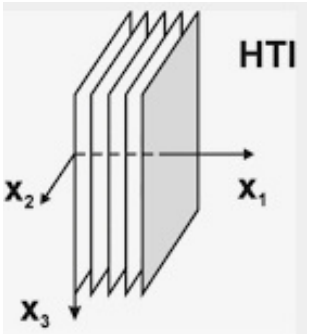

Figure 3: HTI media (Vertical open fractures in isotropic background)

2.3.2 ORT anisotropic model

In Orthorhomic anisotropy, we have three mutually perpendicular planes of symmetry. Two sets of orthogonal fracture in isotropic background or a set of parallel vertical fractures in VTI background could result in such anisotropy.

2.3.3 Monoclinic anisotropic model

If the two sets of vertical fractures embedded in a transversely isotropic rock with vertical axis of symmetry are non-orthogonal, the equivalent medium is monoclinic. Transverse isotropy is usually due to fine horizontal layering and the equivalent medium has a

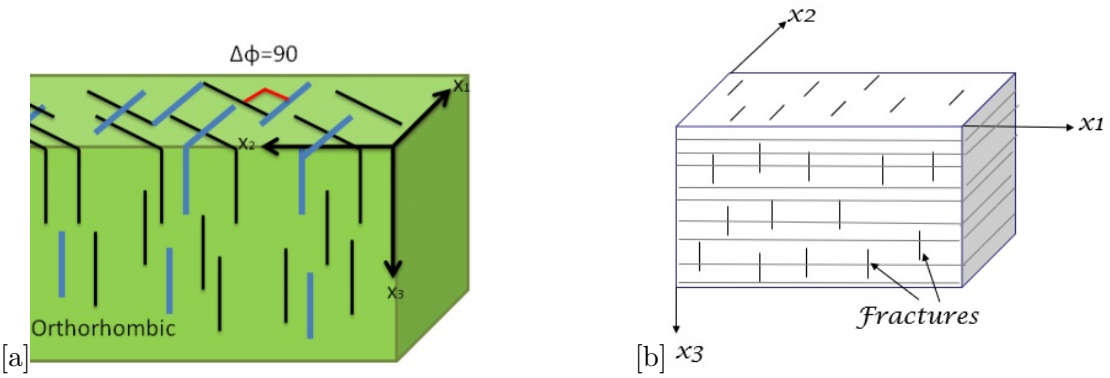

Figure 4: ORT media: a)Orthorhombic symmetry formed by 2 sets of vertical and orthogonal fractures embedded in an isotropic background (Mehdi. E. far et al., 2011) . b)A set of parallel vertical fractures in VTI background

horizontal symmetry plane. Numerous experiments under confined compression show that shear fractures commonly develop in conjugate pairs (Twiss and Moores, 1992). The wide use of monoclinic models in practice may not be quite common but it is often applicable under certain geological scenario (as for example, seismic exploration in strike slip margins of Earth).

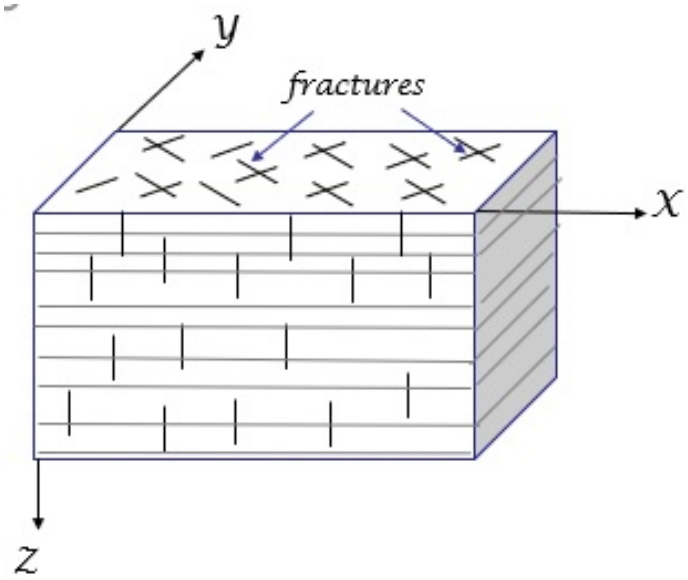

Figure 5: Schematic diagram of 2 sets of long vertical fractures non-orthogonal to each other embedded in a TI medium with a vertical symmetry axis .

3 VFTI media

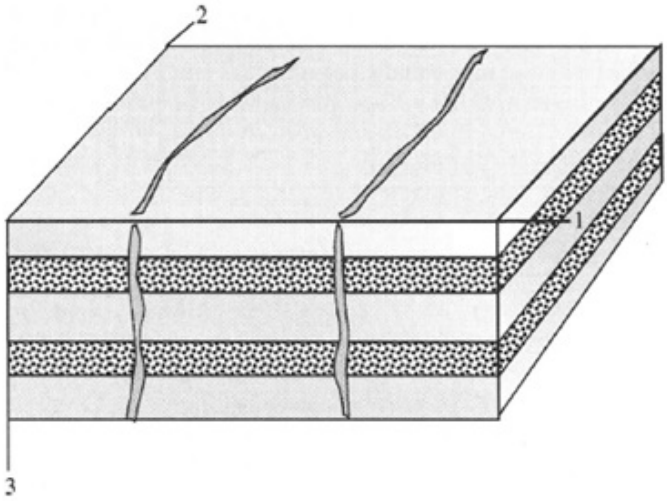

Figure 6: Schematic diagram of long vertical fractures aligned in the 2,3-plane embedded in a TI medium with a vertical symmetry axis (Schoenberg and Helbig, 1997).

VFTI stands for vertically fractured media with transverse isotropy. The x_3 -axis is the axis of symmetry of the background TI medium, usually assumed to be the vertical axis, and the x_1 -axis is normal to the fractures so that we are considering vertical fractures as shown in figure 6 . The x_2 direction is considered to be parallel to the strike of fractures.

3.1 Orthorhombic symmetry

Vertical fractures and horizontal fine layering, under low frequency limit combine to form equivalent orthorhombic (ORT) medium. Orthorhombic symmetry is expected because the earth's anisotropy is dictated by two causes. The first is the regional stress field and the second cause is rock heterogeneity which, in general, implies horizontal stratification. This is quite common in sedimentary rocks like shale.

3.2 Fracture Weaknesses

The orthorhombic elastic stiffnesses of a horizontally stratified medium embedded by a system of parallel vertical fractures can be expressed in terms of the TI background moduli and the excess compliance caused by the fractures. For convenience, a dimensionless quantity calculated from fracture compliances and VTI background stiffness coefficients is defined. This is termed as fracture weakness (equation A.6, Appendix A). Thus, if elastic stiffnesses of an orthorhombic medium can be estimated from seismic data of some sort, one can test whether they satisfy the VFTI constraint. If they do, the stiff-

ness matrix can be decomposed into the stiffnesses of the unfractured background rock and the fracture compliances (Hood and Schoenberg, 1989).

3.3 Equivalent Stiffness coefficients

The stiffnesses of the fracture model are derived from those of a TI background medium combined with a set of fracture compliances. The stiffnesses and compliances of the long-wavelength equivalent homogeneous orthorhombic medium are functions of the five stiffnesses C_{llb} , C_{33b} , C_{44b} , C_{13b} , and C_{66b} of the TI background medium and of the three positive fracture parameters Z_N, Z_H, and Z_V, where Z_N is the excess compliance normal to the fractures, Z_H is the excess horizontal tangential compliance, and Z_V is the excess vertical tangential compliance (Schoenberg and Helbig, 1997).
Equivalent stiffness coefficients(equation A.7, Appendix A) vary linearly with the fracture weaknesses. Plots of equivalent stiffnesses for VFTI media vs fracture weaknesses (fig. 7) are generated using the numerical data provided in section 3.4. In the plots, it can be clearly seen that c_{11e} varies strongly with the change in δ_N. However, there is a little variation in c_{33e} with the fracture weakness δ_N.

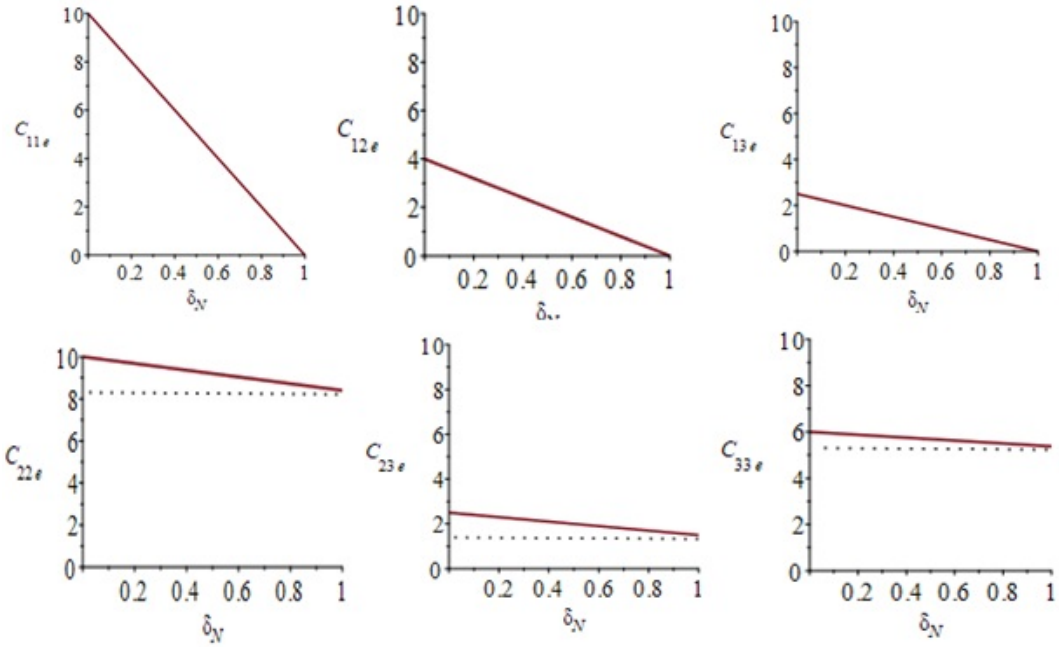

Figure 7: Plots of equivalent stiffnesses for VFTI media vs fracture weakness δ_N

3.4 Numerical data

The numerical values for characterizing the VFTI and monoclinic models for this report are assigned as under (Schoenberg and Helbig, 1997).

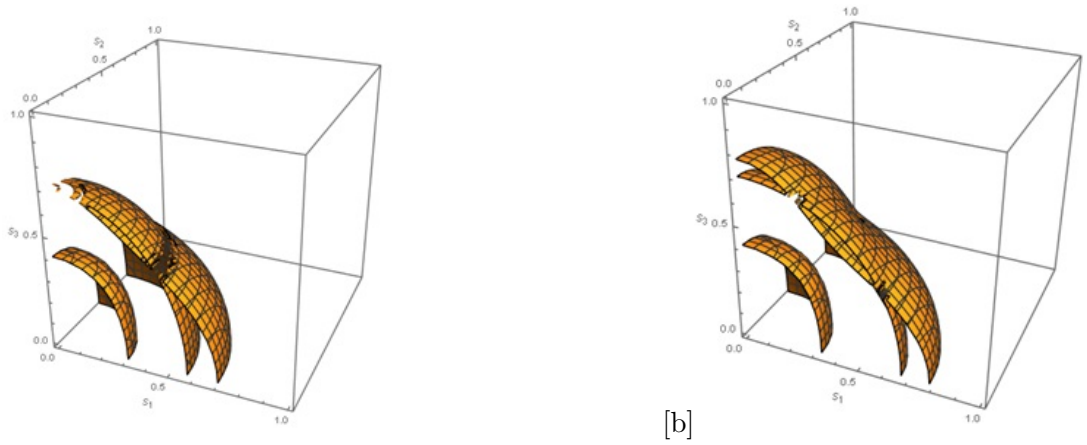

[a] [b]

Figure 8: Slowness surfaces based on the standard model (Schoenberg and Helbig, 1997). a) VTI backgound b) VFTI media

A standard background VTI model typical of shale:

$$C_b = \begin{bmatrix} 10 & 4 & 2.5 & 0 & 0 & 0 \\ 4 & 10 & 2.5 & 0 & 0 & 0 \\ 2.5 & 2.5 & 6 & 0 & 0 & 0 \\ 0 & 0 & 0 & 2 & 0 & 0 \\ 0 & 0 & 0 & 0 & 2 & 0 \\ 0 & 0 & 0 & 0 & 0 & 3 \end{bmatrix} \tag{1}$$

The fracture weaknesses δ_N, δ_V and δ_H as calculated are 0.1, 0.2 and 0.3 respectively. The density-normalized stiffness matrix of the equivalent VFTI medium for the given standard background model is

$$C_e = \begin{bmatrix} 9 & 3.6 & 2.25 & 0 & 0 & 0 \\ 3.6 & 9.84 & 2.4 & 0 & 0 & 0 \\ 2.25 & 2.4 & 5.9 & 0 & 0 & 0 \\ 0 & 0 & 0 & 2 & 0 & 0 \\ 0 & 0 & 0 & 0 & 1.6 & 0 \\ 0 & 0 & 0 & 0 & 0 & 2.2 \end{bmatrix} \tag{2}$$

3.5 Slowness surface for VFTI media

The slowness surface for VFTI media is computed from the standard model (Appendix B). The dotted lines are slowness surfaces for VTI background and the Solid ones represent that for VFTI media (figure 9). The magnitude of slowness, in general increases due to fracturing. The slowness surface for the P-wave is less affected than the slowness surfaces for S waves by the presence of vertical fractures. Concavity in the slowness surface of S_V wave is more for VFTI media (as seen in symmetry planes) than VTI

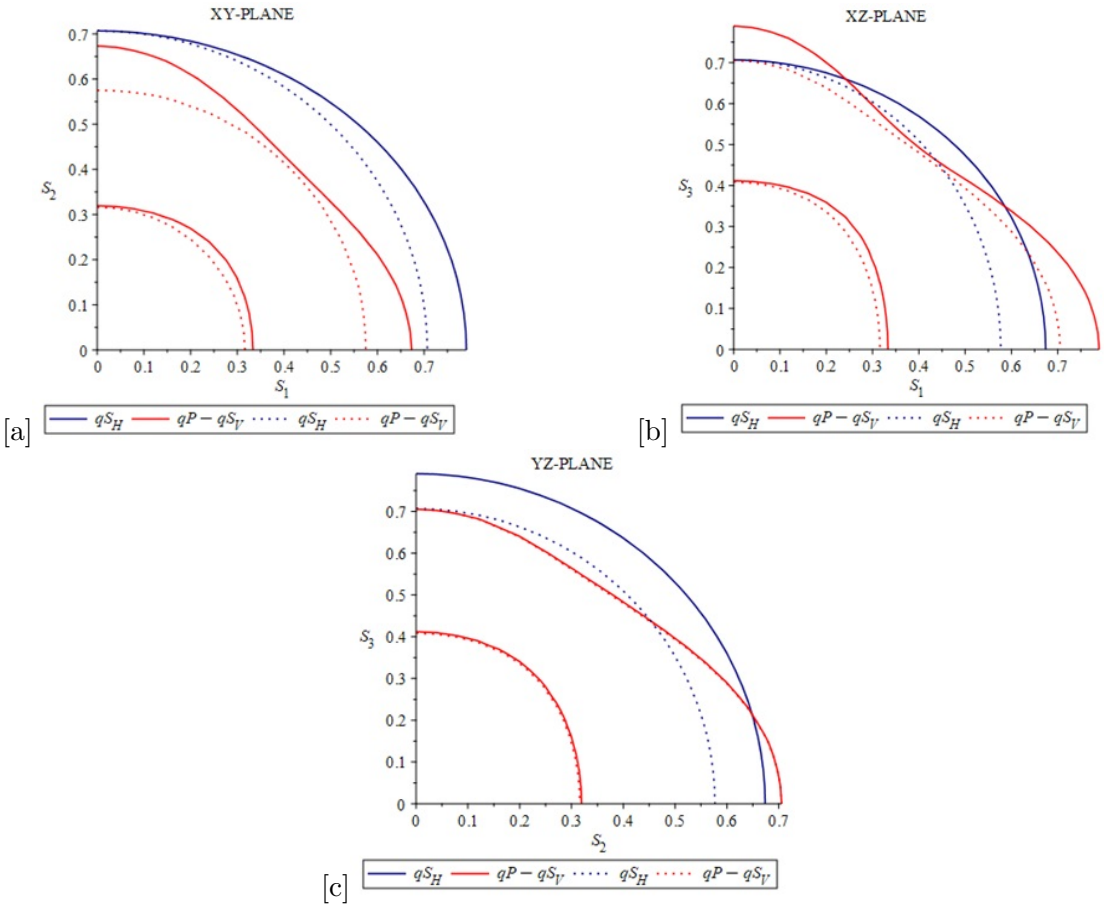

Figure 9: Slowness surfaces in the symmetry planes. a) XY-plane b) XZ-plane c)YZ-plane.

background media. The slowness surfaces for P and S_V waves are very less affected in the YZ- symmetry plane (which is parallel to the fracture plane).

4 Monoclinic media

4.1 Monoclinic symmetry

Monoclinic medium with a horizontal symmetry plane consists of two nonorthogonal sets of long, thin vertical fractures in VTI background. It is widely presented in various seismic applications: moveout approximations for P, S_1 and S_2 waves (Farra et al., 2016), inversion of monoclinic parameters to fracture parameters (Bakulin et al., 2000), and reflection and transmission coefficients at the plane interface between two half-spaces of monoclinic symmetry (Song and Stovas, 2020).

4.2 Equivalent Stiffness coefficients

The stiffnesses of the fracture model are derived from those of a TI background medium combined with two sets of fracture compliances. The stiffness coefficients of the homogeneous monoclinic medium thus are functions of the five stiffnesses C_{11b} , C_{33b} , C_{44b} , C_{13b} , and C_{66b} of the TI background medium, two sets of positive fracture compliances (K_N, K_H, and K_V) and azimuth angles of fracture sets, where K_N is the excess compliance normal to the fractures, K_H is the excess horizontal tangential compliance, and K_V is the excess vertical tangential compliance (Schoenberg and Helbig, 1997). The azimuth angles of fracture sets ϕ_1 and ϕ_2 are measured as the angles between corresponding fracture normals (fr_{n1} and fr_{n2}) and X-axis.

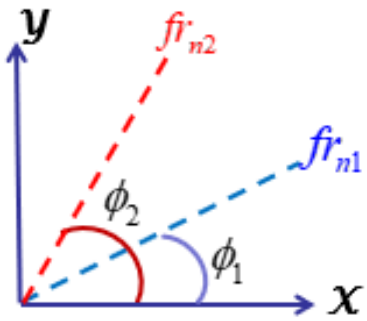

Figure 10: Azimuth angles of fracture sets for monoclinic model

Equivalent stiffness coefficients of the monoclinic model has been derived in Appendix E . Compared to the ORT/VFTI model with nine independent stiffness coefficients, the monoclinic model has four additional independent stiffness coefficients, namely c_{16}, c_{26}, c_{36} and c_{45}.

5 NMO velocity ellipse

The NMO velocity ellipse plays an important role in seismic data processing and analysis because this is one of the most stable parameter to estimate. The NMO velocity should not be confused to propagation velocity. In anisotropic model, it is related to the curvature of the group velocity surface at the vertical axis (Stovas, 2021). Normal move-out (NMO) velocities can be calculated from the traveltime parameters for different wave modes.

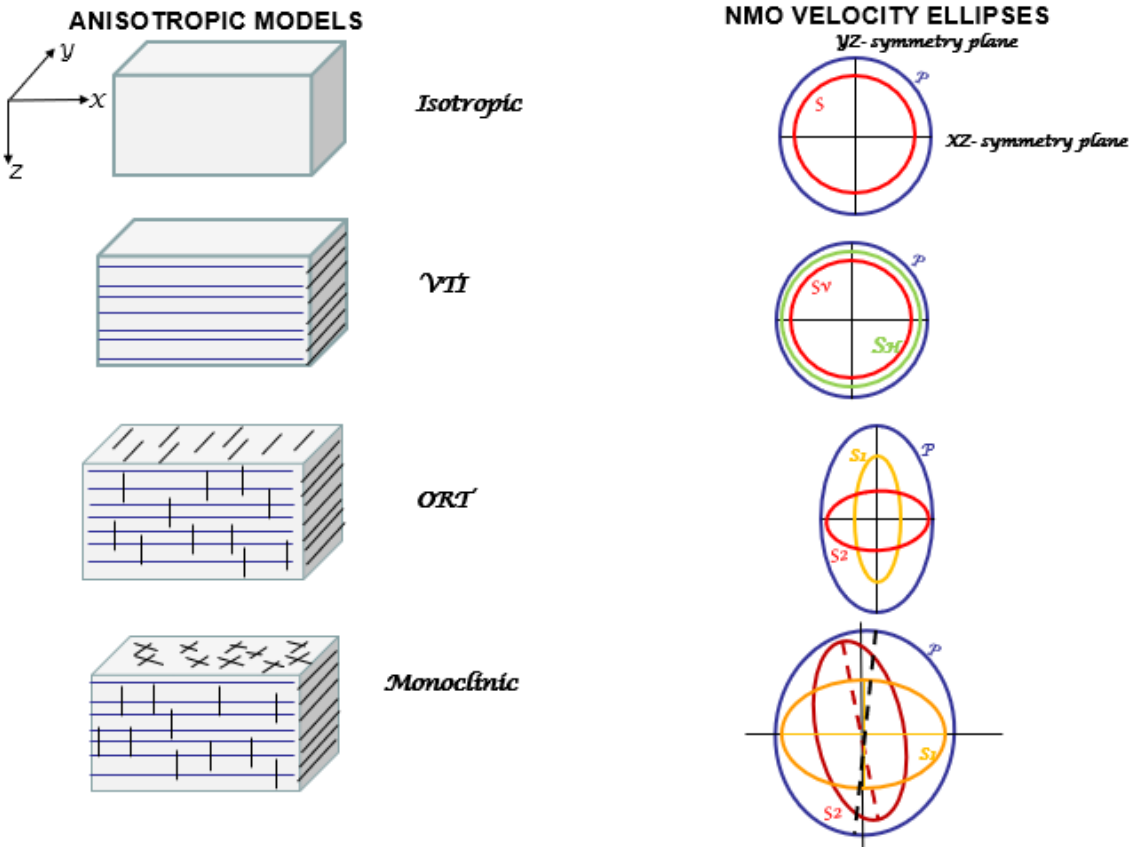

Figure 11: NMO velocity ellipse surfaces for anisotropic models

The magnitude of normal-moveout velocity is same in all azimuthal direction for isotropic and VTI media and so the NMO velocity surface is circle. The two NMO velocity surfaces or circles for isotropic media represents P wave (larger radius) and S wave (smaller radius). For the VTI media, we have three such circles corresponding to P, S_V and S_H waves. For the VFTI media (that possesses orthorhombic symmetry), the orientation of major axis of the NMO ellipse gives the strike of fracture set. However, in case of monoclinic media, the orientation of ellipses can be rotated randomly depending on the azimuth angles of fracture sets. For orthorhombic and monoclinic media, we have NMO

velocity ellipses for P, S_1 and S_2 waves.

5.1 NMO ellipse for orthorhombic media

The elements of the Christoffel's matrix can be given as

$$\Gamma = \begin{bmatrix} \Gamma_{11} & \Gamma_{12} & \Gamma_{13} \\ \Gamma_{12} & \Gamma_{22} & \Gamma_{23} \\ \Gamma_{13} & \Gamma_{23} & \Gamma_{33} \end{bmatrix} \tag{3}$$

It can be represented in terms of density normalised stiffness coefficients and unit velocity vectors.
For orthorhombic medium,
$\Gamma_{11} = c_{11}n_1^2 + c_{66}n_2^2 + c_{55}n_3^2$
$\Gamma_{12} = (c_{12} + c_{66})n_1n_2$
$\Gamma_{13} = (c_{13} + c_{55})n_1n_3$
$\Gamma_{22} = c_{66}n_1^2 + c_{22}n_2^2 + c_{44}n_3^2$
$\Gamma_{23} = (c_{23} + c_{44})n_2n_3$
$\Gamma_{33} = c_{55}n_1^2 + c_{44}n_2^2 + c_{33}n_3^2$

where, $n_1 = sin\theta cos\phi$, $n_2 = sin\theta sin\phi$, $n_3 = cos\theta$
and the equation for NMO velocities ellipse can be written as,

$$V_{nmo}^2 = V_1^2 cos^2\phi + V_2^2 sin^2\phi \tag{4}$$

, where ϕ is measured from the x_1 direction. V_1 and V_2 are normal move-out velocities in XZ and YZ-symmetry planes respectively.

$$V^2 = V_0^2 + [V_1^2 cos^2\phi + V_2^2 sin^2\phi - V_0^2]sin^2\theta \tag{5}$$

, where θ is measured from the normal to the interface and V_0 is the vertical propagation velocity of wave.

$$F = \mid \Gamma - I.V \mid \tag{6}$$

, where I is the 3 x 3 identity matrix.
The solution of F gives the values for NMO velocities. When $\theta = 0$, we only have vertical propagation of waves. The obtained solutions are c_{33}, c_{44} and c_{55} representing P, S_1 and S_2 wave squared velocities respectively. Likewise, by adjusting the values of V_0 , θ and ϕ, we get NMO velocities for different wave modes in XZ-symmetry plane and YZ-symmetry plane.

5.1.1 Eccentricity of the ellipse

Eccentricity of the ellipse is given by the ratio of squared NMO velocities in XZ-symmetry plane over YZ-symmetry plane.

$$e' = \sqrt{1 - \frac{V_1^2}{V_2^2}} \tag{7}$$

, where $V_2 > V_1$

For practical purpose in this study, eccentricity

$$e = \frac{V_1^2}{V_2^2} = f(c_{ijb}, \delta_N, \delta_V, \delta_H) \tag{8}$$

Eccentricity of the NMO ellipse for VFTI media is a function of the VTI background stiffnesses and fracture weaknesses. Therefore, it can be linearized in terms of fracture weaknesses.

5.1.2 NMO ellipse for VFTI model

VFTI model has orthorhombic symmetry due to presence of a set of parallel vertical fractures in the VTI background. If we have wave propagation in VTI medium, then the NMO velocities are same over all azimuthal direction. So, the NMO velocity surface can be represented by a circle with $V_1 = V_2$, where V_1 and V_2 are NMO velocities in XZ and YZ symmetry planes respectively. However, if we have orthorhombic or monoclinic anisotropy, then this surface is no longer a circle but an ellipse. In such cases, V_1 and V_2 are different.

A two layered model (figure no. 12) consisting of the upper VFTI layer and the lower VTI layer separated by an interface is considered. The background of the VFTI media is assumed to be the same as that of lower VTI layer. If a P wave is incident at the interface, the reflected wave can be a P or S waves. Considering all possible combination to examine NMO velocity ellipses in VFTI media, we have following wave modes:

Pure wave modes PP, S_1S_1, S_2S_2 and converted wave modes PS_1, PS_2, S_1S_2.

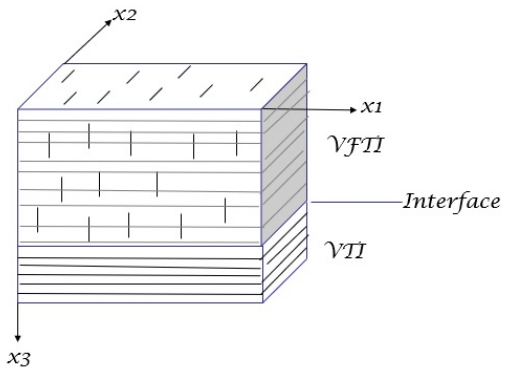

Figure 12: Two layered model with VFTI media over VTI

5.2 Eccentricity for different wave modes

5.2.1 Analyses for sensitivities towards fracture weaknesses

Sensitivities are the coefficients infront of fracture weaknesses in the equation of squared NMO velocities linearized in terms of fracture weaknesses. This equation consist of fractured and unfractured part. The sensitivities are thus function of background stiffnesses.

$$V_j^2 = V_b^2 + A_{\delta_N,j}\delta_N + A_{\delta_V,j}\delta_V + A_{\delta_H,j}\delta_H \tag{9}$$

j= 1,2. V_b = NMO Velocity for unfractured background.
Here $A_{\delta,j} = f(c_{ijb}); i,j = 1,2,...,6$ are sensitivities.

$$V_j^2 = V_b^2(1 + A^{\sim}_{\delta_N,j}\delta_N + A^{\sim}_{\delta_V,j}\delta_V + A^{\sim}_{\delta_H,j}\delta_H) \tag{10}$$

j= 1,2.
Here $A^{\sim}_{\delta,j} = A_{\delta,j}/V_b^2; i,j = 1,2.$ is a dimensionless quantity referred as normalized (with respect to background medium squared NMO velocity) sensitivities. The sensitivities of NMO velocities ellipse's eccentricity towards fracture weaknesses for different wave modes (figure 13) are described as below:
PP - The sensitivity towards δ_V is much higher than towards δ_N in XZ-symmetry plane. The sensitivity towards δ_H is zero.
S_1S_1 - The sensitivity towards δ_V is again higher than towards δ_N in XZ-symmetry plane. The sensitivity towards δ_H is lower than for other fracture weaknesses and δ_H sensitivity is only in YZ-symmetry plane.
S_2S_2 - The sensitivity towards δ_V is zero and is very small value for δ_N. So, the squared NMO velocity for this wave mode is mainly sensitive to δ_H.
PS_1 - The sensitivity towards δ_N is again higher than towards δ_V and δ_H in XZ-symmetry plane. δ_H sensitivity is only in YZ-symmetry plane. The sensitivity towards δ_V is lower than for other fracture weaknesses.
PS_2 - The squared NMO velocity for this wave mode is sensitive to all the fracture weaknesses. The sensitivity towards δ_V is higher than for other fracture weaknesses.
S_1S_2 - The squared NMO velocity for this wave mode is sensitive to all the fracture weaknesses. The sensitivity towards δ_H is dominant factor here as it has significant equal value in both XZ and YZ symmetry planes.
The graphical representation for these sensitivities based on the standard model are given in Appendix C.

5.3 NMO ellipse for monoclinic media

For monoclinic model with a horizontal symmetry plane,
$\Gamma_{11} = c_{11}n_1^2 + c_{66}n_2^2 + c_{55}n_3^2 + 2c_{16}n_1n_2$
$\Gamma_{12} = c_{16}n_1^2 + c_{26}n_2^2 + c_{45}n_3^2 + (c_{12} + c_{66})n_1n_2$
$\Gamma_{13} = (c_{13} + c_{55})n_1n_3 + (c_{36} + c_{45})n_2n_3$
$\Gamma_{22} = c_{66}n_1^2 + c_{22}n_2^2 + c_{44}n_3^2 + 2c_{26}n_1n_2$

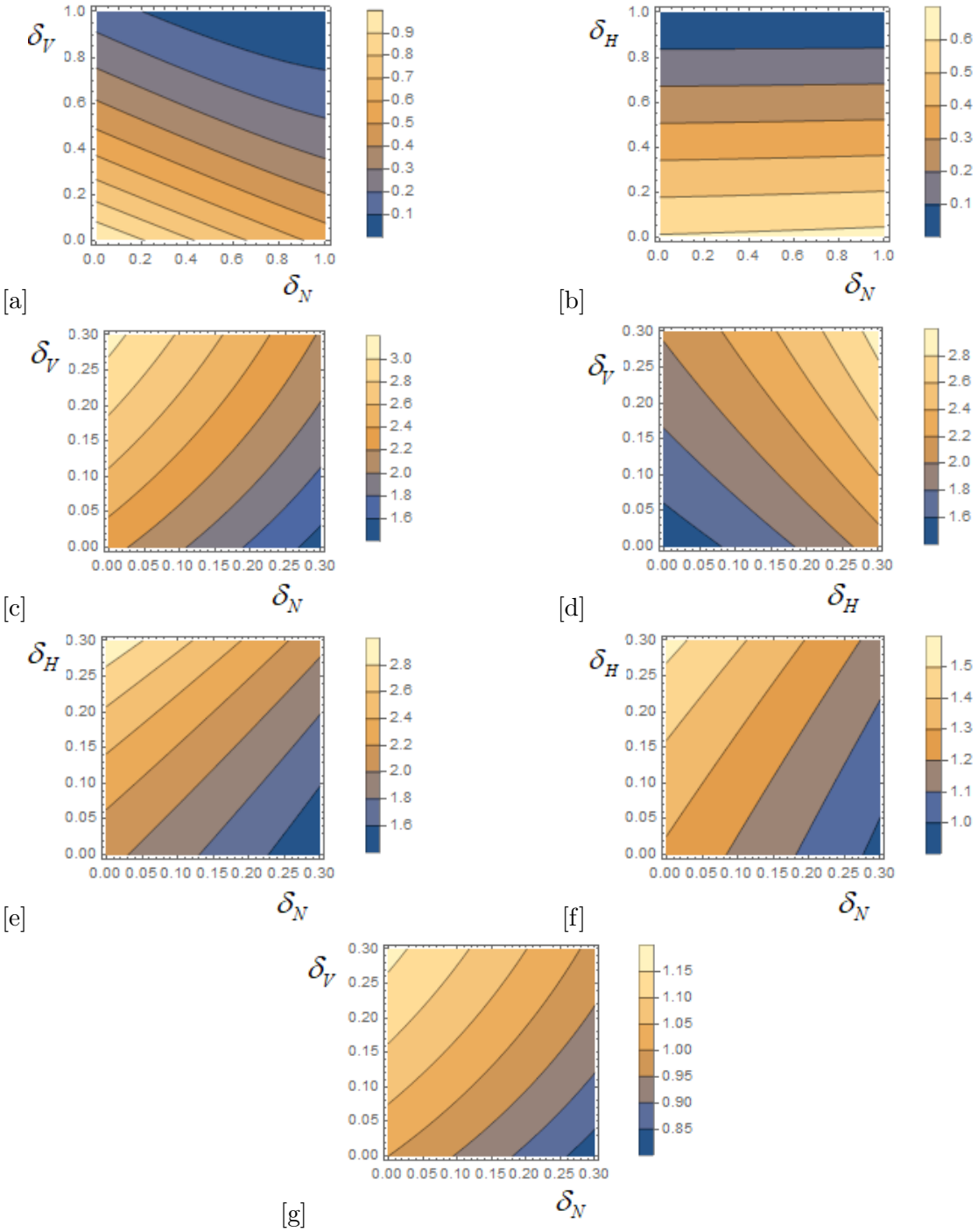

Figure 13: Variation of eccentricities with fracture weaknesses for different wave modes a) e_{PP} b) $e_{S_2S_2}$ c) $e_{S_1S_1}(\delta_N - \delta_V)$ d) $e_{S_1S_1}(\delta_V - \delta_H)$ e) $e_{S_1S_1}(\delta_N - \delta_H)$ f) e_{PS_1} g) $e_{S_1S_2}$

$\Gamma_{23} = (c_{23} + c_{44})n_2n_3 + (c_{36} + c_{45})n_1n_3$
$\Gamma_{33} = c_{55}n_1^2 + c_{44}n_2^2 + c_{33}n_3^2 + 2c_{45}n_1n_2$

where, $n_1 = sin\theta cos\phi$, $n_2 = sin\theta sin\phi$, $n_3 = cos\theta$

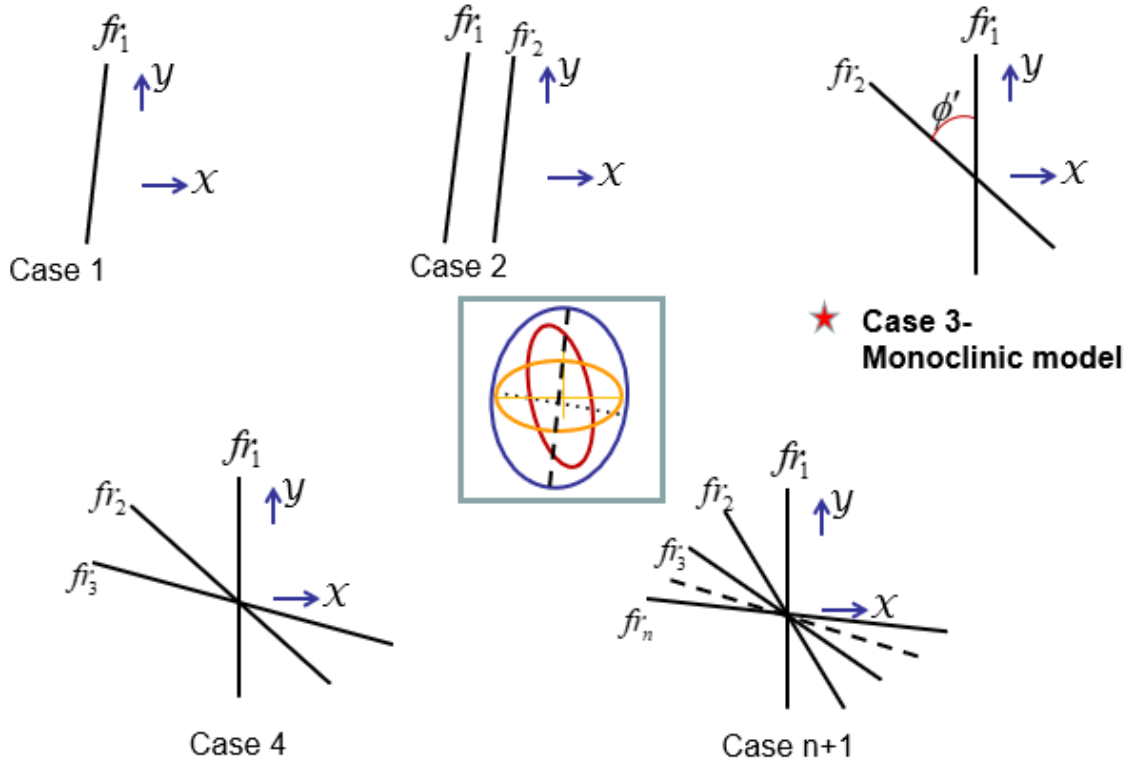

Figure 14: Possible cases of fracture systems in VTI background that may give similar NMO velocity ellipses

If we are given NMO velocity ellipses for P, S_1 and S_2 waves (represented by blue, yellow and red colours respectively in figure 14), it is quite possible to predict the orientation of the fracture systems present in a transversely isotropic rock with vertical axis of symmetry. In the figure, we can infer several possible cases of fracture systems from the given NMO velocity ellipses. fr_1, fr_2,... fr_n are fracture sets. $\phi^{'}$ is the angle between two non-orthogonal fracture sets in case 3 and the overall effective media has monoclinic symmetry. One can utilize core sample/geological or other type of lab data to confirm the most probable case.

5.3.1 NMO phase velocity ellipse

The equation for the phase velocity squared has the following form:

$$v^2(\theta,\phi) = v_0^2 + [v_{nmo}^2(\phi) - v_0^2]sin^2\theta + O(sin^4\theta) \tag{11}$$

,where

$$v_{nmo}^2(\phi) = a_{20}cos^2\phi + 2a_{11}sin\phi cos\phi + a_{02}sin^2\phi \tag{12}$$

with v_0 being the vertical phase velocity and coefficients a_{20}, a_{11} and a_{02} define the NMO phase-velocity ellipse.

The coefficients can be found by selecting the proper v_0. c_{33}, c_{44} and c_{55} represent squared vertical phase velocities for P, S_2 and S_1 wave respectively. For the P-wave, the coefficients are given by

$$\begin{aligned} a_{20} &= \frac{(c_{13}+c_{55})^2 + c_{55}(c_{33}-c_{55})}{c_{33}-c_{55}} + \frac{c_{36}^2}{c_{33}-c_{44}} \\ a_{02} &= \frac{(c_{23}+c_{44})^2 + c_{44}(c_{33}-c_{44})}{c_{33}-c_{44}} + \frac{c_{36}^2}{c_{33}-c_{55}} \\ a_{11} &= c_{36}\left(\frac{c_{13}+c_{55}}{c_{33}-c_{55}} + \frac{c_{23}+c_{44}}{c_{33}-c_{44}}\right) \end{aligned} \tag{13}$$

For the S_1-wave,

$$\begin{aligned} a_{20} &= \frac{-(c_{13}+c_{55})^2 + c_{11}(c_{33}-c_{55})}{c_{33}-c_{55}} \\ a_{02} &= c_{66} - \frac{c_{36}^2}{c_{33}-c_{55}} \\ a_{11} &= \frac{c_{16}(c_{33}-c_{55}) - c_{36}(c_{13}+c_{55}}{c_{33}-c_{55}} \end{aligned} \tag{14}$$

For the S_2-wave,

$$\begin{aligned} a_{20} &= c_{66} - \frac{c_{36}^2}{c_{33}-c_{44}} \\ a_{02} &= \frac{-(c_{23}+c_{44})^2 + c_{22}(c_{33}-c_{44})}{c_{33}-c_{44}} \\ a_{11} &= \frac{c_{26}(c_{33}-c_{44}) - c_{36}(c_{23}+c_{44}}{c_{33}-c_{44}} \end{aligned} \tag{15}$$

The $P-$, S_1, and S_2- wave monoclinic anisotropy parameters (Stovas, 2021) responsible for rotation of the corresponding NMO phase-velocity ellipses are respectively defined

as

$$\begin{aligned}
\xi_3 &= \frac{(a_{11})_P}{2v_o^2} = \frac{c_{36}}{2c_{33}}\left(\frac{c_{13}+c_{55}}{c_{33}-c_{55}} + \frac{c_{23}+c_{44}}{c_{33}-c_{44}}\right) \\
\xi_1 &= \frac{(a_{11})_{S1}}{2v_o^2} = \frac{c_{16}(c_{33}-c_{55}) - c_{36}(c_{13}+c_{55}}{2c_{55}(c_{33}-c_{55})} \\
\xi_2 &= \frac{(a_{11})_{S2}}{2v_o^2} = \frac{c_{26}(c_{33}-c_{44}) - c_{36}(c_{23}+c_{44}}{2c_{44}(c_{33}-c_{44})}
\end{aligned} \tag{16}$$

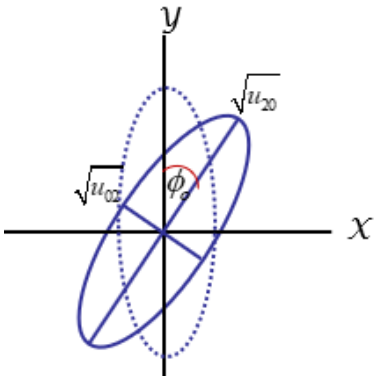

Figure 15: NMO ellipse with arbitrarily oriented axes

The NMO phase-velocity equation can be rewritten as

$$v_{nmo}^2(\phi) = u_{20}cos^2(\phi-\phi_o) + u_{02}sin^2(\phi-\phi_o) \tag{17}$$

where ϕ_o is the rotation angle of NMO ellipse measured from Y-axis and the ellipse semiaxes $\sqrt{u_{20}}$ and $\sqrt{u_{02}}$ can be related to coefficients a_{20}, a_{11} and a_{02} as:

$$u_{20}, u_{02} = \frac{1}{2}\left(a_{20}+a_{02} \pm \sqrt{(a_{20}-a_{02})^2 + 4a_{11}^2}\right), \tag{18}$$

$$tan2\phi_o = \frac{2a_{11}}{a_{20}-a_{02}} \tag{19}$$

The above two equations are helpful in establishing NMO phase-velocity coefficients from a given NMO ellipse with random orientation (fig.15) . This is important to make NMO velocity data applicable for inversion to fracture parameters. On simple comparison of equation 12 with equation 17, one can get the NMO phase-velocity coefficients,

$$\begin{aligned}
a_{20} &= u_{20}cos^2(\phi_o) + u_{02}sin^2(\phi_o) \\
a_{02} &= u_{20}sin^2(\phi_o) + u_{02}cos^2(\phi_o) \\
a_{11} &= (u_{20}-u_{02})sin(\phi_o)cos(\phi_o)
\end{aligned} \tag{20}$$

This type of assessment is also applicable to NMO group velocity and NMO group-velocity coefficients can be similarly obtained from the measurements of axes and rotation angle of random NMO group ellipse. In practice, we measure traveltime of any event with the help of source-receiver system and so our calculations are mostly performed in group domain. In this context, the next section is focused on understanding the NMO group ellipses for P and S waves in detail.

5.3.2 NMO group velocity ellipse

The inverse group velocity squared is given by the equation:

$$\frac{1}{V^2(\Theta,\Phi)} = \frac{1}{V_0^2} + \left[\frac{1}{V_n^2(\Phi)} - \frac{1}{V_0^2}\right] sin^2\Theta + O(sin^4\Theta) \tag{21}$$

,where

$$\frac{1}{V_n^2(\Phi)} = A_{20}cos^2\Phi + 2A_{11}sin\Phi cos\Phi + A_{02}sin^2\Phi \tag{22}$$

with V_0 being the vertical group velocity, Θ and Φ being group polar incident and azimuth angles and coefficients A_{20}, A_{11} and A_{02} define the NMO group-velocity ellipse.

The group velocity coefficients A_{ij} can be computed from coefficients a_{ij} defined for different wave modes in equations 13-15 (Grechka et al., 1999):

$$\begin{aligned} A_{20} &= \frac{a_{02}}{a_{20}a_{02} - a_{11}^2} \\ A_{02} &= \frac{a_{20}}{a_{20}a_{02} - a_{11}^2} \\ A_{11} &= -\frac{a_{11}}{a_{20}a_{02} - a_{11}^2} \end{aligned} \tag{23}$$

The group-velocity coefficients can be linearized in terms of fracture weaknesses of the two fracture sets. Since fracture weaknesses are small quantities, higher order terms can be neglected.
$A_{ij} = f_1.\delta_{N1} + f_2.\delta_{V1} + f_3.\delta_{H1} + f_4.\delta_{N2} + f_5.\delta_{V2} + f_6.\delta_{H2}$
$f_1, ..., f_6 = f(c_{ijb}, \phi_n)$,
where ϕ_n is azimuth angle of fracture set 'n' with n=1,2 and i,j=1,...,6

5.3.3 Analyses of NMO group ellipses with respect to fracture parameters

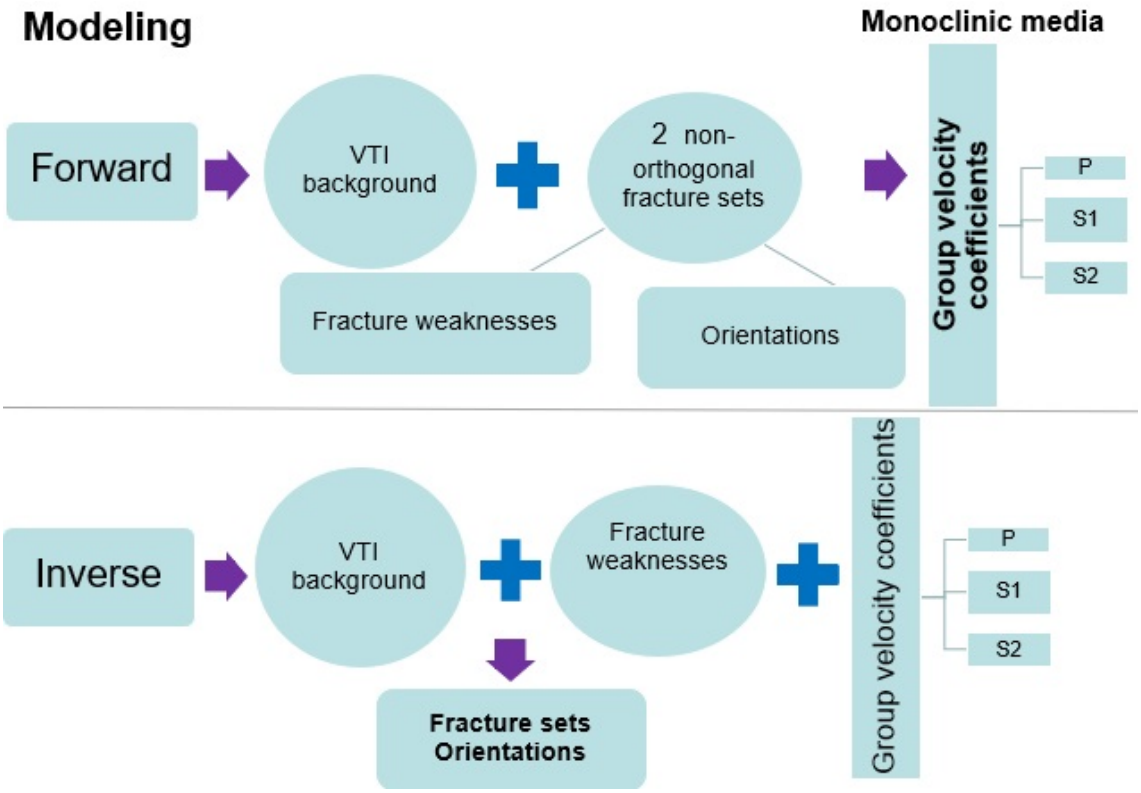

Figure 16: Methodology to analyze NMO group ellipse response to fractures

I have considered two modeling studies, namely forward and inverse. In the forward modeling, NMO group velocity ellipses for P, S_1 and S_2 waves are obtained using background stiffness coefficients and information about fracture sets, i.e., fracture weaknesses and azimuth angles. The group velocity coefficients A_{20}, A_{11} and A_{02} are calculated from NMO phase velocity coefficients a_{20}, a_{11} and a_{02} using the relation as mentioned in equation 23. These calculations are made for two different cases of fracture weaknesses of fracture sets: Case 1: The fracture weaknesses for both fracture sets are identical. Case 2: The fracture weaknesses of one fracture set is different from the other. The details of cases and calculations for a standard model are given in Table 4 and Table 5.

In the inverse modeling, the azimuth angles of the fracture sets are determined from the given NMO group velocity ellipses for P, S_1 and S_2 waves. The VTI background and fracture weaknesses information are known and considered the same to the ones used for forward modeling. Here again, the analyses have been done for the two above mentioned cases of fracture weaknesses values of fracture sets. To determine the orientations of fracture sets, I used one of the NMO group velocity coefficients (A_{20}, A_{11} or A_{02}) at a time for pair of wave modes ($P - S_1$, $P - S_2$ and $S_1 - S_2$).

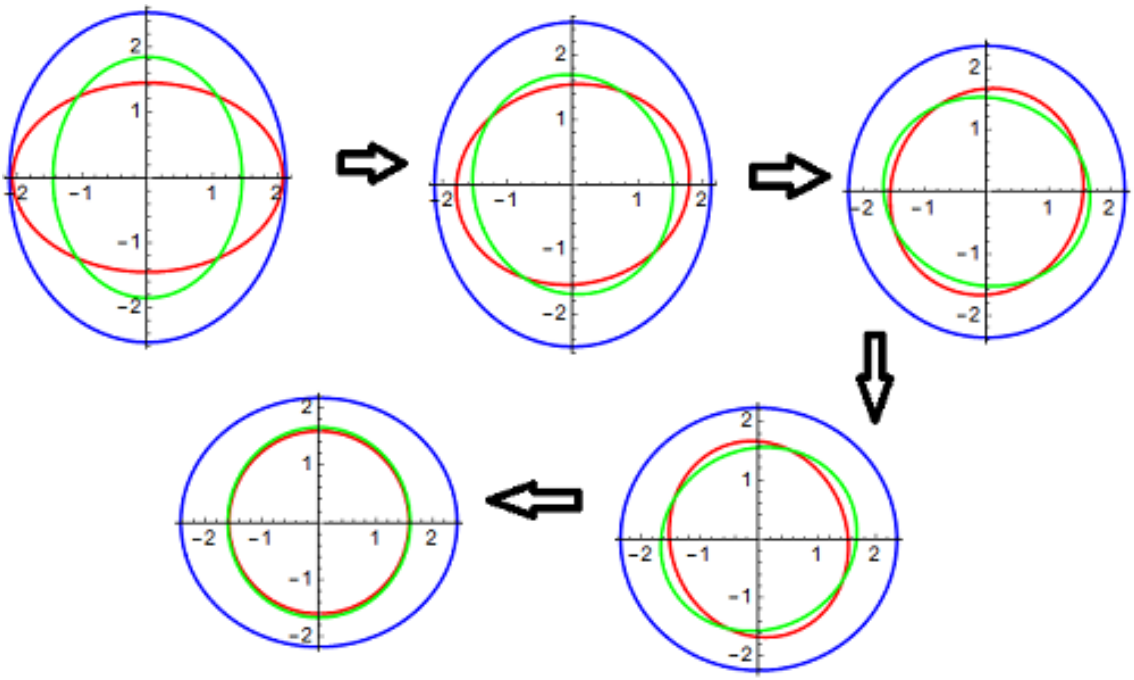

Figure 17: Variation of NMO group ellipses with orientation of fracture sets

NMO group velocity ellipses for P, S_1 and S_2 waves are shown in figure no. 17. The blue, red and green colours correspond respectively to P, S_1 and S_2 waves. The polar azimuth angle varies from 0 to 360 degrees. Initially the angle $\phi^{'}$ between normal to fracture set 1 and normal to fracture set 2 are considered small and gradually this angle is increased such that $\phi^{'} \in (0°, 90°)$. The direction of arrows marks this increase of angle. Here, changes in the shape and size of ellipses are clearly visible. Shear wave is more sensitive to fracture as compared to Primary body wave.

Variation of Group velocity coefficients with orientation of fracture sets
The NMO group velocity coefficients (A_{20}, A_{11} and A_{02}) were computed for P, S_1 and S_2 wave modes in terms of background stiffness coefficients, fracture weaknesses and azimuth angles for fracture sets. The standard VTI background stiffness matrix, typical of shale rock(Schoenberg and Helbig, 1997) was used. The azimuth angles, ϕ_1 varies from 0 to 90° and ϕ_2 varies from 0 to $-90°$. To study this variation, two cases were taken into account,
Case 1: when the fracture weaknesses of both fracture sets are identical,
$\delta_{N1} = \delta_{N2} = 0.1$
$\delta_{V1} = \delta_{V2} = 0.2$
$\delta_{H1} = \delta_{H2} = 0.3$

Case 2: when the fracture weaknesses of fracture sets are non-identical,

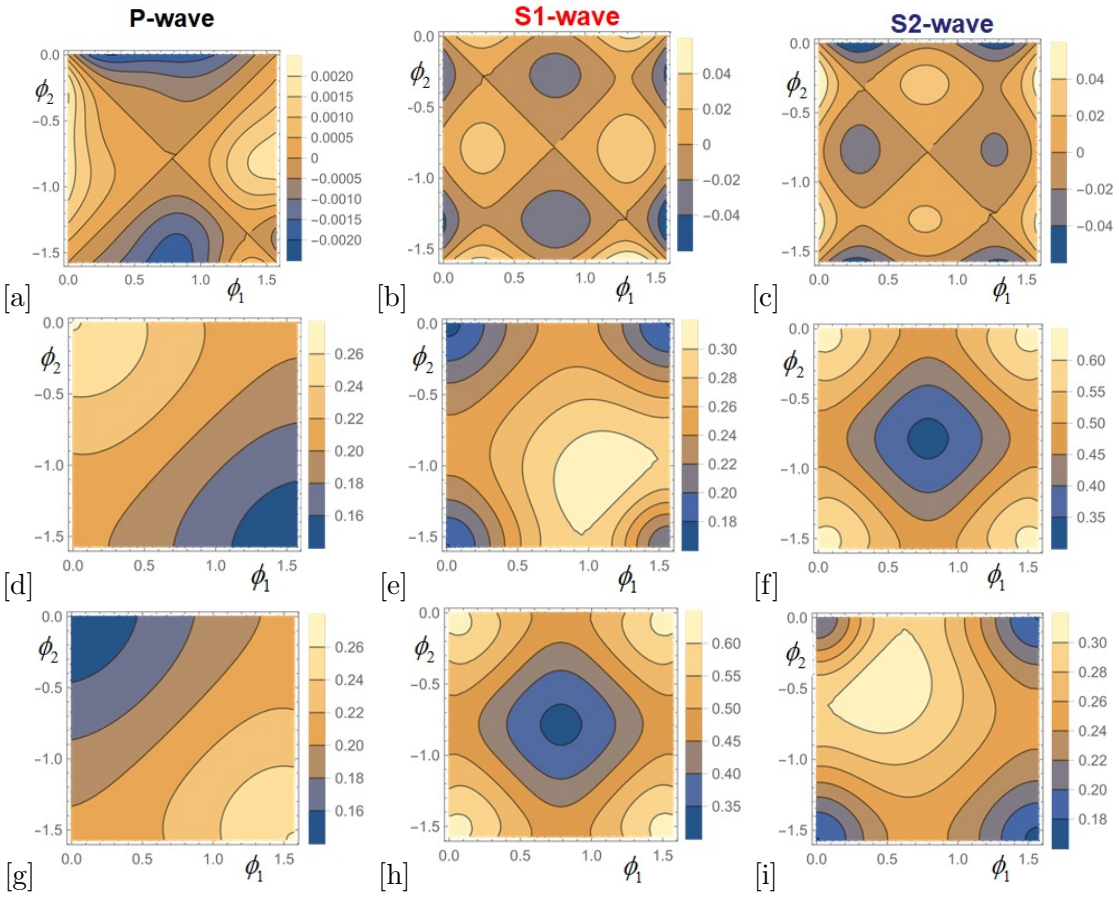

Figure 18: Variation of NMO Group Velocity coefficients with azimuth angles of fracture sets (a, b, c) A_{11} ; (d, e, f) A_{20} ; (g, h, i) A_{02} for P, S_1 S_2 waves respectively

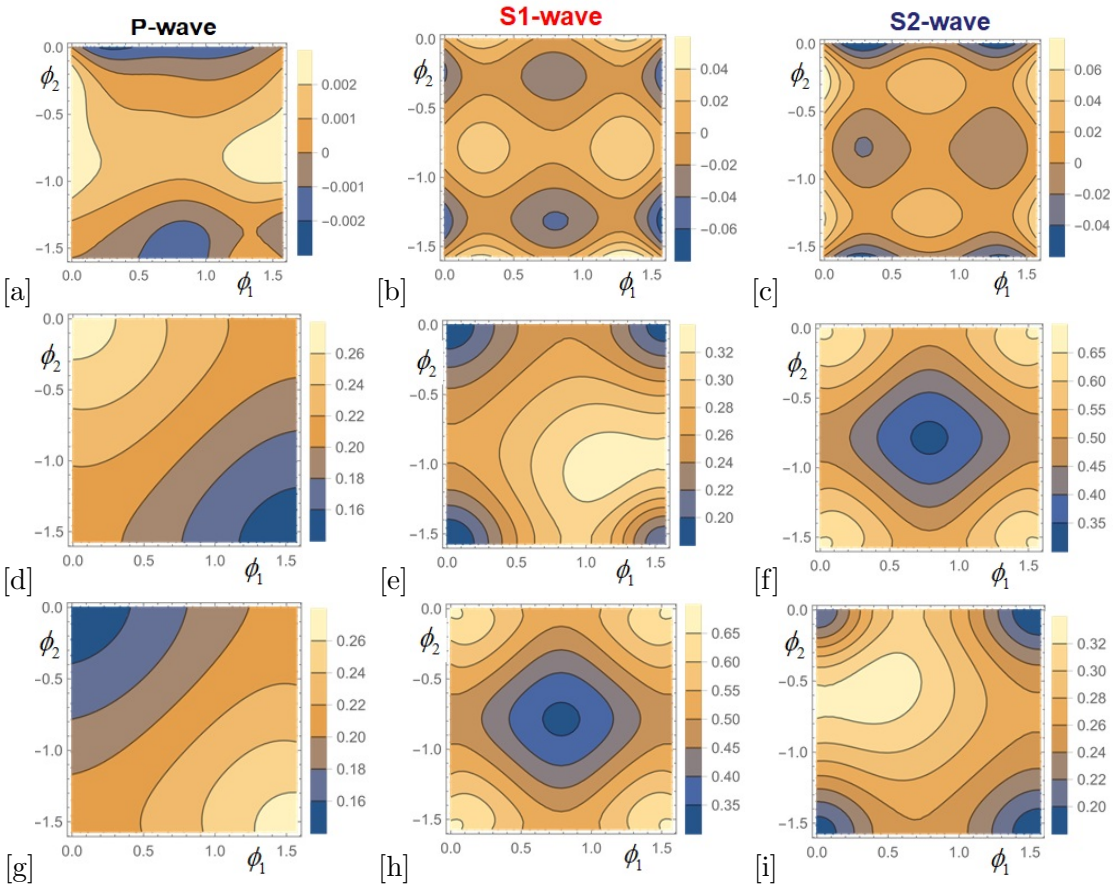

Figure 19: Plot of NMO Group Velocity coefficients vs azimuth angles when fracture sets are not identical (a, b, c) A_{11} ; (d, e, f) A_{20} ; (g, h, i) A_{02}

In this case,
$\delta_{N1} = 0.1, \delta_{N2} = 0.15$
$\delta_{V1} = 0.2, \delta_{V2} = 0.2$
$\delta_{H1} = 0.3, \delta_{H2} = 0.35$
Also, one can notice that the magnitude of fracture weaknesses for fracture set 2 has been increased. Due to the loss of symmetry around X-axis in the horizontal plane, the pattern of curves has also changed. This means considerable changes in the NMO group ellipse.

Sensitivity analysis towards fracture weaknesses
For this study, fracture weakness values of both fracture sets are assumed to be identical i.e.,
$\delta_{N1} = \delta_{N2} = \delta_N$
$\delta_{V1} = \delta_{V2} = \delta_V$

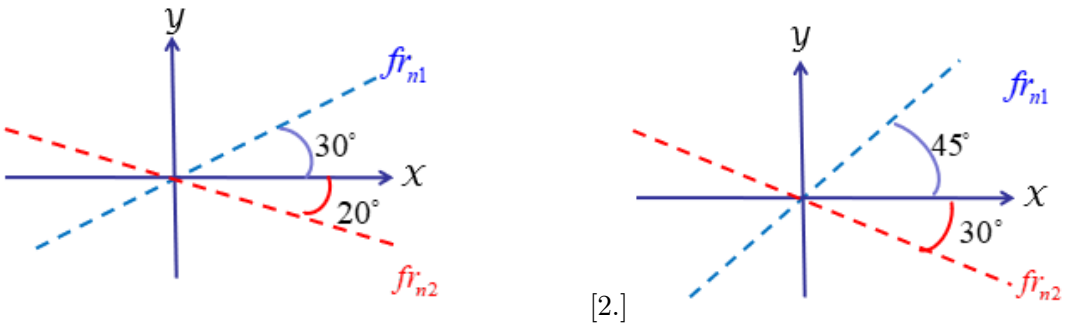

Figure 20: Orientation of fracture systems in horizontal plane. Angle between normals to two fracture sets are 1) small 2) relatively large

$\delta_{H1} = \delta_{H2} = \delta_H$
and two different orientations of fracture systems are considered. Here, fr_{n1} and fr_{n2} are normals to the fracture set 1 and 2 respectively. The azimuth angles measured from X-axis has been shown in the figure 20. The variation of NMO group velocity coefficient A_{11} for P, S_1 and S_2 waves with fracture weaknesses for two different orientation cases are shown in figure 21.

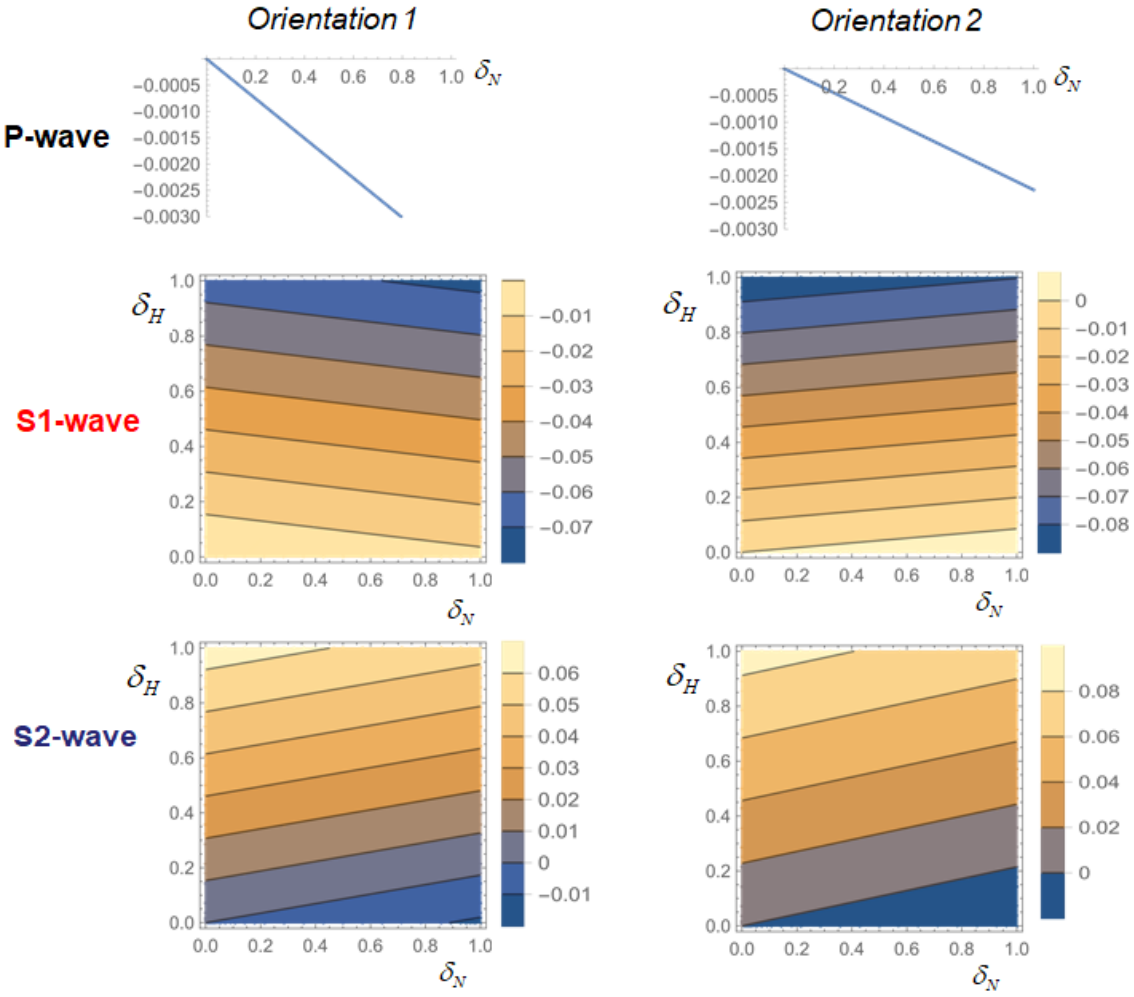

Figure 21: Variation of A_{11} with fracture weaknesses for two different orientations of fracture systems

6 Amplitude vs azimuth data-set

Variations of reflection amplitude with azimuth are sensitive to the presence of natural and induced fractures. The gradient terms in the reflection coefficients of amplitude vs azimuth (AVAz) attribute can be analyzed for this variation. This analysis gives us two information related to the sensitivities to the fractures:
a) How different orientations of fracture sets are responsible for this variation. Which fracture weaknesses affects the reflection coefficient's gradient most for a particular wave mode. b) How is the variation in the magnitude of gradient in different direction or with azimuth angle ϕ.

6.1 Reflection coefficient (Pure and converted waves)

The reflection coefficient is the proportion of seismic wave amplitude reflected from an interface to the wave amplitude incident upon it. The reflection coefficient depends on the impedance of a rock layer. The impedance is defined as the product of bulk density ρ and wave velocity V.
Reflection coefficient for reflection form the interface between two layers namely upper layer 1 and lower layer 2 can be given as,

$$R = \frac{Z_2 - Z_1}{Z_2 + Z_1} \tag{24}$$

, where $Z_1 = \rho_1 V_1$ and $Z_2 = \rho_2 V_2$

The reflection coefficient for pure wave modes[34] can be written as

$$R(\theta, \phi) = R_0 + G(\phi) sin^2\theta \tag{25}$$

Here, R_0 = Intercept
G = Gradient
θ = Incident angle for wave modes
ϕ = Polar azimuth angle measured from x-axis in horizontal plane

The reflection coefficient for converted wave modes can be written as

$$R(\theta, \phi) = G(\phi) sin\theta \tag{26}$$

Here, G = Gradient

6.2 AVAz gradient-VFTI media

To obtain the gradient terms in the reflection coefficients of amplitude vs azimuth, AVAz dataset for different wave modes, a two layer model (fig. 22) is considered. The upper layer is VTI and the lower layer is VFTI media. The VTI background of the VFTI layer

is same as the upper VTI layer. This means the background stiffnesses of the VFTI layer are same as that of VTI layer. There is reflection from the interface between two layers.

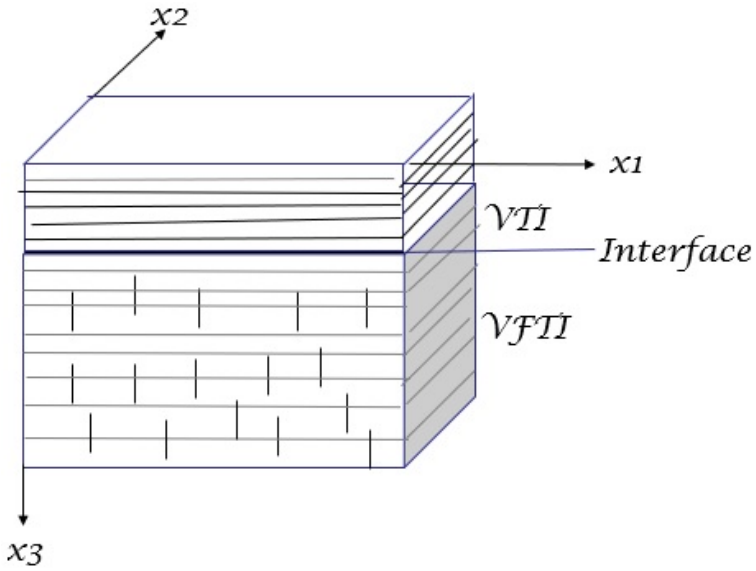

Figure 22: Two layered model with VTI over VFTI media

The reflection coefficients for pure and converted wave modes in such a model are utilized (Song and Stovas, 2020) to get gradients.

6.2.1 Cases for two sets of Fracture weaknesses

To observe the sensitivities towards fracture weaknesses of the AVAz gradients, two sets of fracture weaknesses are defined.
The set 1 is represented by f1 and set 2 by f2.

f= $(\delta_N, \delta_V, \delta_H)$
f1 = (0.1 , 0.2 , 0.3)
f2 = (0.15 , 0.3 , 0.4)

Here, it can be seen that the magnitude of fracture weaknesses have increased and so do the extent of fracturing.

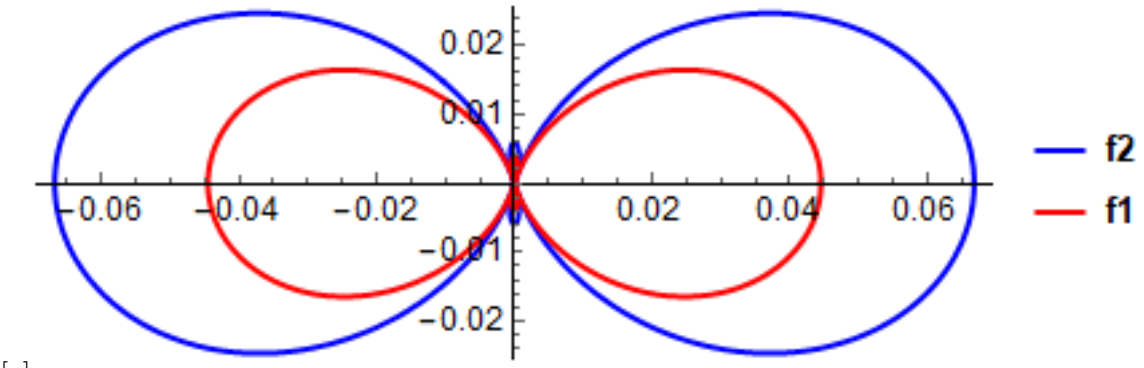

[a]

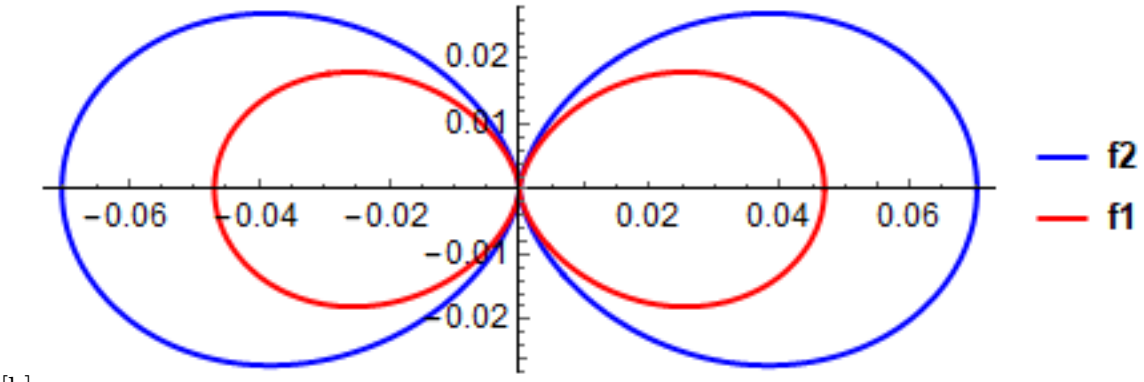

[b]

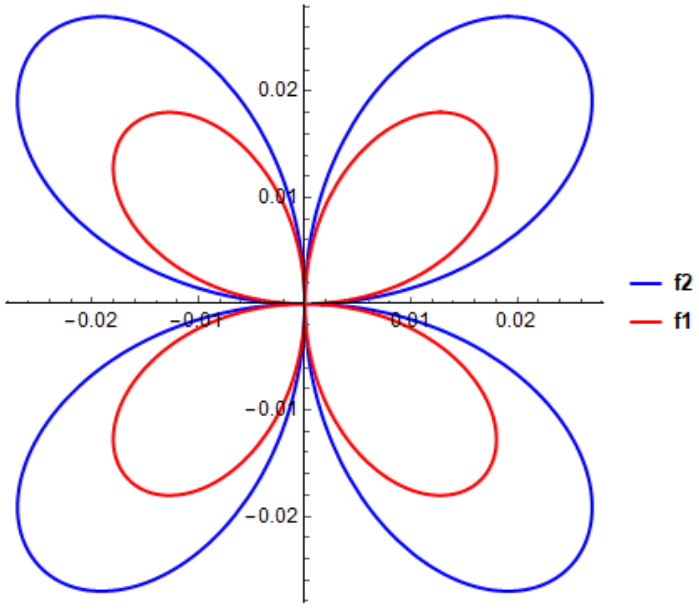

[c]

Figure 23: Variation of AVAz gradient (for different sets of fracture weaknesses) with polar azimuth angle. a)$G_{PP}(\phi)$ b) $G_{P-S_V}(\phi)$ c)$G_{P-S_H}(\phi)$

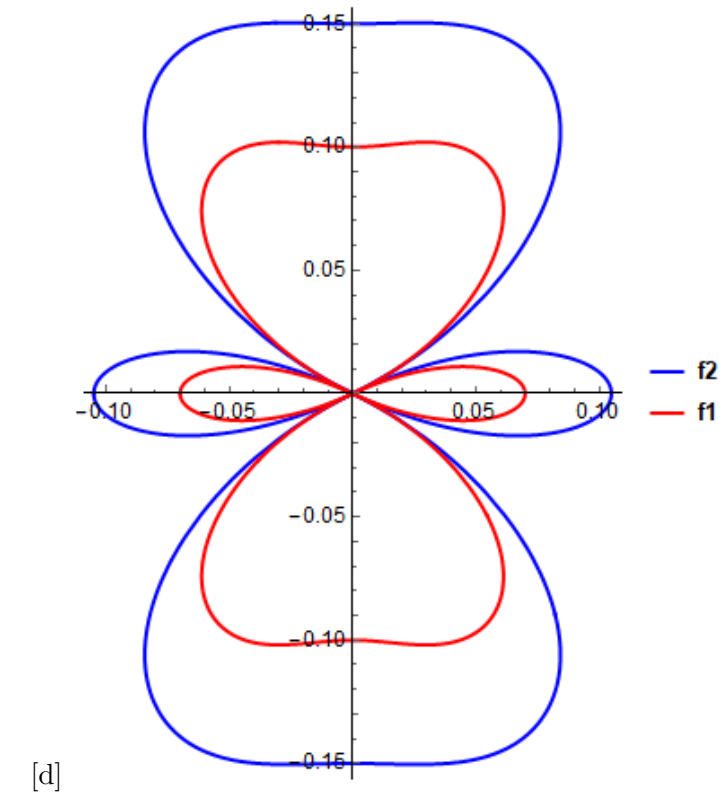

[d]

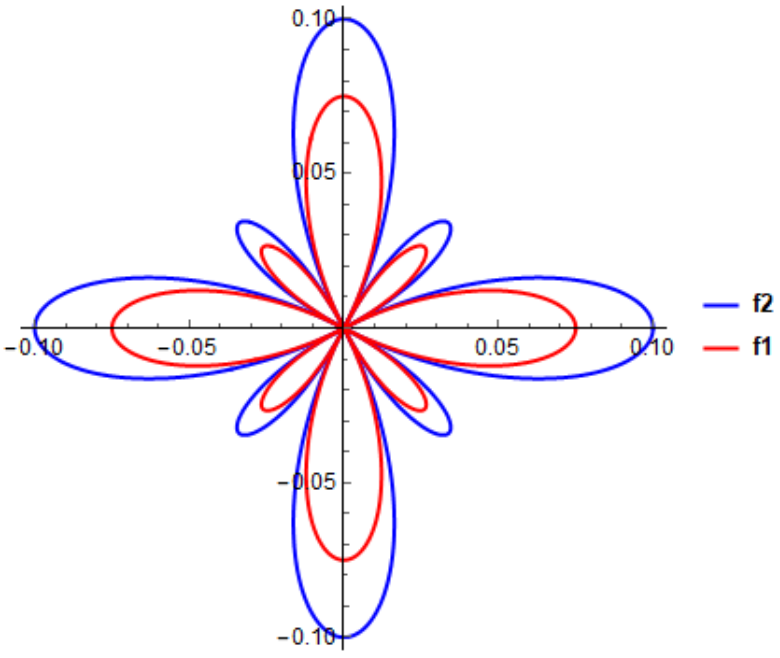

[e]

Figure 23: Variation of AVAz gradient (for different sets of fracture weaknesses) with polar azimuth angle. d)$G_{S_V-S_V}(\phi)$ e)$G_{S_H-S_H}(\phi)$. ϕ varies from 0° to 360°

6.2.2 Analyses for sensitivities towards fracture weaknesses

The change in the values of gradient of reflection coefficients for different wave modes are different depending on the function of the phase angle ϕ. Here, ϕ varies from 0 to 360 degrees. Also, one can notice from the plots that the change in the magnitude of the gradients vary with direction. The sensitivities are numerically given by the coefficients in front of the fracture weaknesses, which is represented by the terms containing constant ζ (Appendix F). The sensitivities of AVAz gradient towards fracture weaknesses for different wave modes are described as below:
PP - The sensitivity towards δ_V is much higher than towards δ_N. The sensitivity towards δ_H is zero.
$S_V - S_V$ - The sensitivity towards δ_V is again higher than towards δ_N . The sensitivity towards δ_H is lower than for other fracture weaknesses.
$S_H - S_H$ - The sensitivity towards δ_V is zero and is very small value for δ_N. So, the AVAz gradient for this wave mode is mainly sensitive to δ_H.
$P - S_V$ - The sensitivity towards δ_V is higher than towards δ_N and towards δ_H is zero.
$P - S_H$ - The sensitivity towards δ_V is higher than towards δ_N.

6.3 AVAz gradient-monoclinic media

The 2-layered model (fig. 24) considered for amplitude vs azimuth analyses consists of VTI media at the top and monoclinic media at the bottom separated by a plane interface. There is reflection from the interface between two layers.

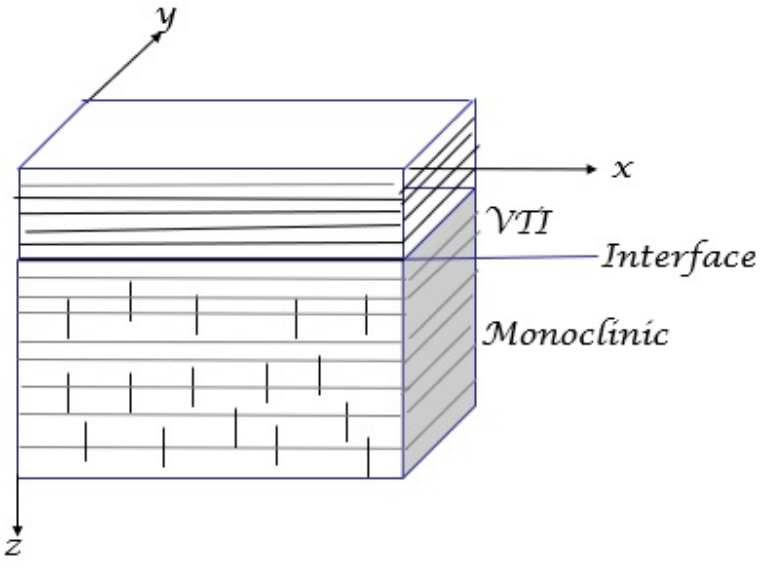

Figure 24: Two layered model with VTI over monoclinic media

Some assumptions have been made to study the AVAz response from this model. Firstly, the VTI background of monoclinic media is same as the top VTI layer. This means that stiffness coefficients of the VTI background of bottom layer are same as the stiffnesses of the top layer. The volume of fracture spaces is infinitesimal, so the density values are nearly equal for both layers. Secondly, the incident angles for P and S waves are small and the ray used to show wave propagation (fig. 25) is closer to the normal at the interface.

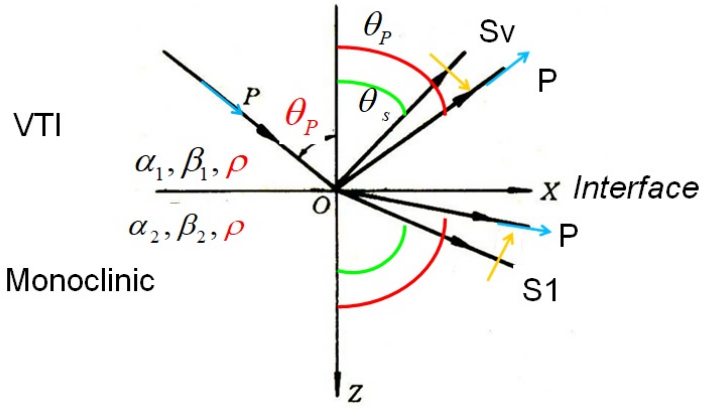

Figure 25: Reflection and transmission of wave modes at the interface

The contrast in the parameters and the average parameters are given as:
$\Delta c_{ij} = (c_{ij})_{monoclinic} - (c_{ij})_{VTI}$,
$\overline{c_{ij}} = \frac{(c_{ij})_{monoclinic} + (c_{ij})_{VTI}}{2}$
with $i, j = 1, 2, ..., 6$.
, where $(c_{ij})_{monoclinic} = f[(c_{ij})_{VTI}, \phi_1, \phi_2, \delta_{N1}, \delta_{V1}, \delta_{H1}, \delta_{N2}, \delta_{V2}, \delta_{H2}]$
The reflection coefficients for pure and converted wave modes in such a monoclinic model are utilized (Song and Stovas, 2020) to get gradients.

6.3.1 Gradients for two different orientations of fracture systems

Once again, the two different orientation cases for fracture systems as shown in figure no. 20 has been taken into account. The fracture weaknesses of both fracture sets are identical with the values,
$\delta_{N1} = \delta_{N2} = 0.1$
$\delta_{V1} = \delta_{V2} = 0.2$
$\delta_{H1} = \delta_{H2} = 0.3$
In the figure 26, blue curve represents gradient corresponding to orientation no. 1 and red curve represents gradient corresponding to orientation no. 2 for fracture systems. Here, polar azimuth angle ϕ varies from 0 to 360°.

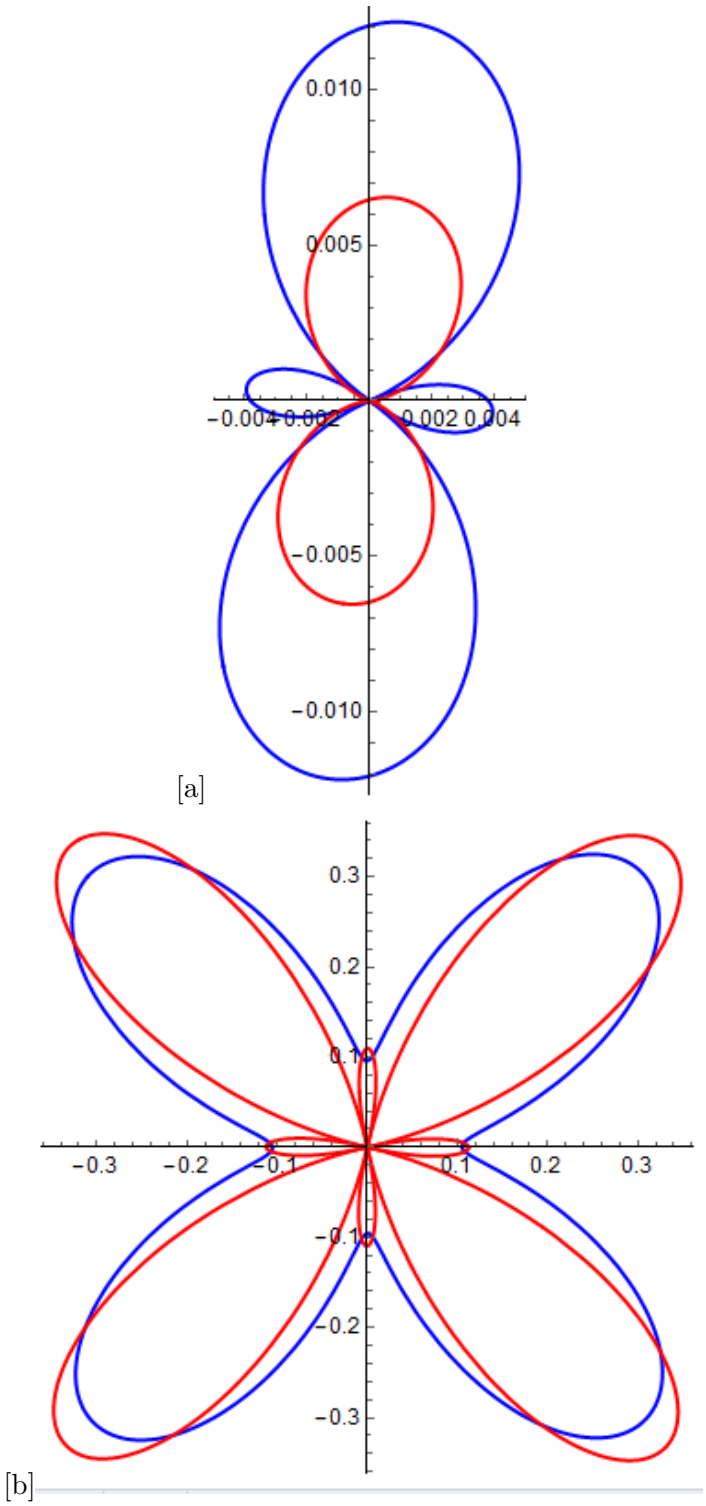

Figure 26: Variation of AVAz gradient term (for different orientations of fracture sets) with polar azimuth angle. a)$G_{PP}(\phi)$ b) $G_{S_V-S_V}(\phi)$.

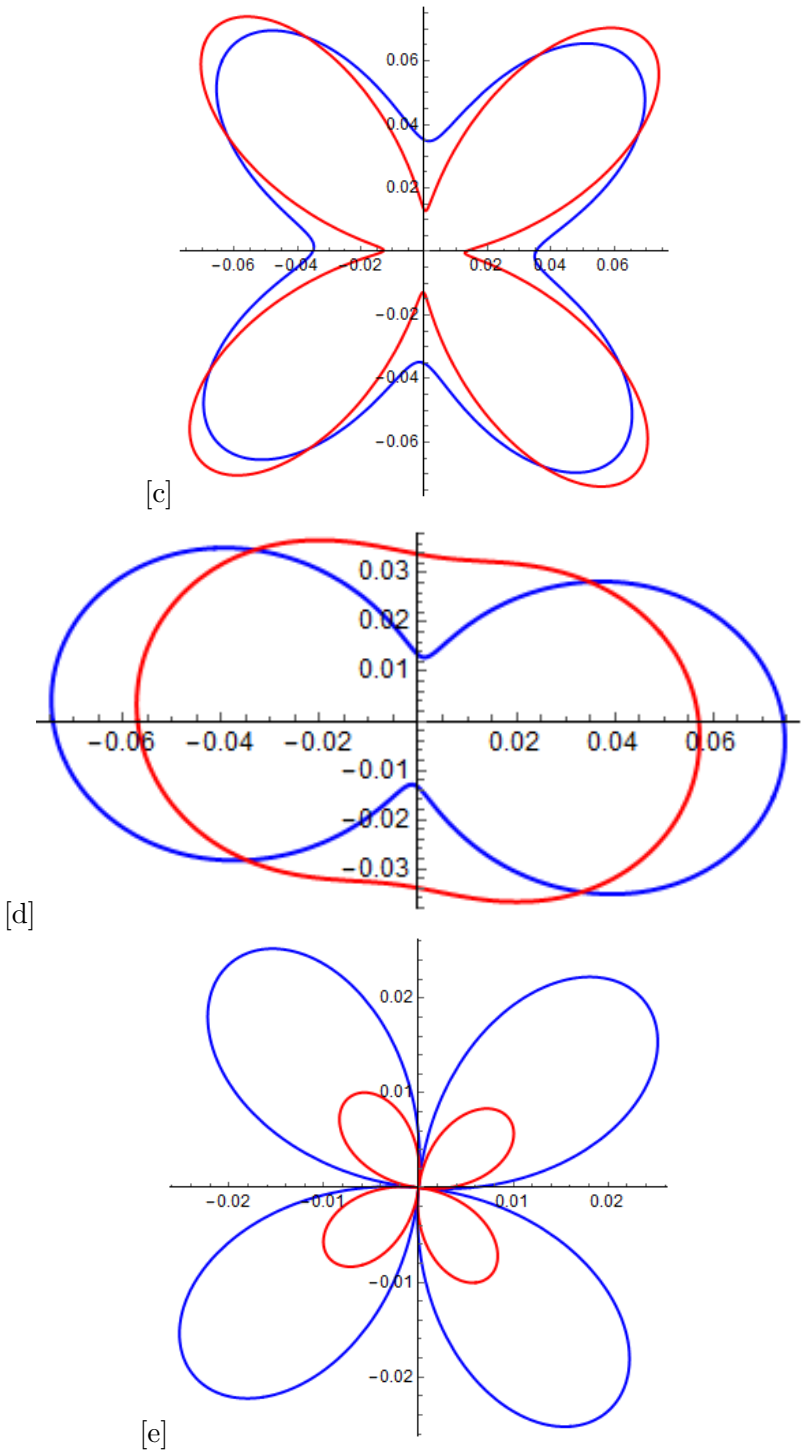

Figure 26: Variation of AVAz gradient term (for different orientations of fracture sets) with polar azimuth angle. c)$G_{S_H-S_H}(\phi)$ d)$G_{P-S_V}(\phi)$ e)$G_{P-S_H}(\phi)$.

6.3.2 Cases for identical and non-identical sets of fracture weaknesses

To understand the sensitivity of gradient terms in the reflection coefficients for different wave modes towards fracture weaknesses, two different cases have been considered. The orientation of fracture sets are fixed in both cases, and orientation no. 1 of figure 20 is utilized for the purpose of calculations.
Case 1: The fracture weaknesses of both fracture sets are identical,
$\delta_{N1} = \delta_{N2} = 0.1$
$\delta_{V1} = \delta_{V2} = 0.2$
$\delta_{H1} = \delta_{H2} = 0.3$
The blue curve in figure 27 defines the gradient corresponding to this case of fracture weaknesses.
Case 2: The fracture weaknesses of fracture sets are non-identical and the magnitude of fracturing has been increased for one of the fracture sets,
$\delta_{N1} = 0.1, \delta_{N2} = 0.15$
$\delta_{V1} = 0.2, \delta_{V2} = 0.2$
$\delta_{H1} = 0.3, \delta_{H2} = 0.35$
The red curve (fig. 27) defines the gradient corresponding to this case of fracture weaknesses. Here, polar azimuth angle ϕ varies from 0 to 360°.

6.3.3 Analyses of response in gradient terms to fracture parameters

It can be noticed that changes in orientation of fracture systems strongly affect the reflection amplitude of the wave modes. Also, the same is true for changes in the magnitude of fracture weaknesses. However, the reflection coefficient's gradients for wave modes $P - S_H$ and $S_H - S_H$ are not changed significantly by slightly changing the fracture weakness values for given monoclinic model. For PP- wave mode, the major change in gradient value is observed at 0° and 90° azimuth angles. For $S_V - S_V$ and $S_H - S_H$, such characteristics changes are observed at 45° azimuth as well apart from 0° and 90°. For converted wave mode $P - S_V$, such conclusion can not be made easily and may depend on VTI background of the model. For converted wave mode $P - S_H$, there are high variations in gradient of AVAz data at 45° azimuth angle. I would like to stress on the symmetric nature of AVAz gradient curves with respect to azimuth angles and so these results are similarly valid for corresponding angles in other quadrants.

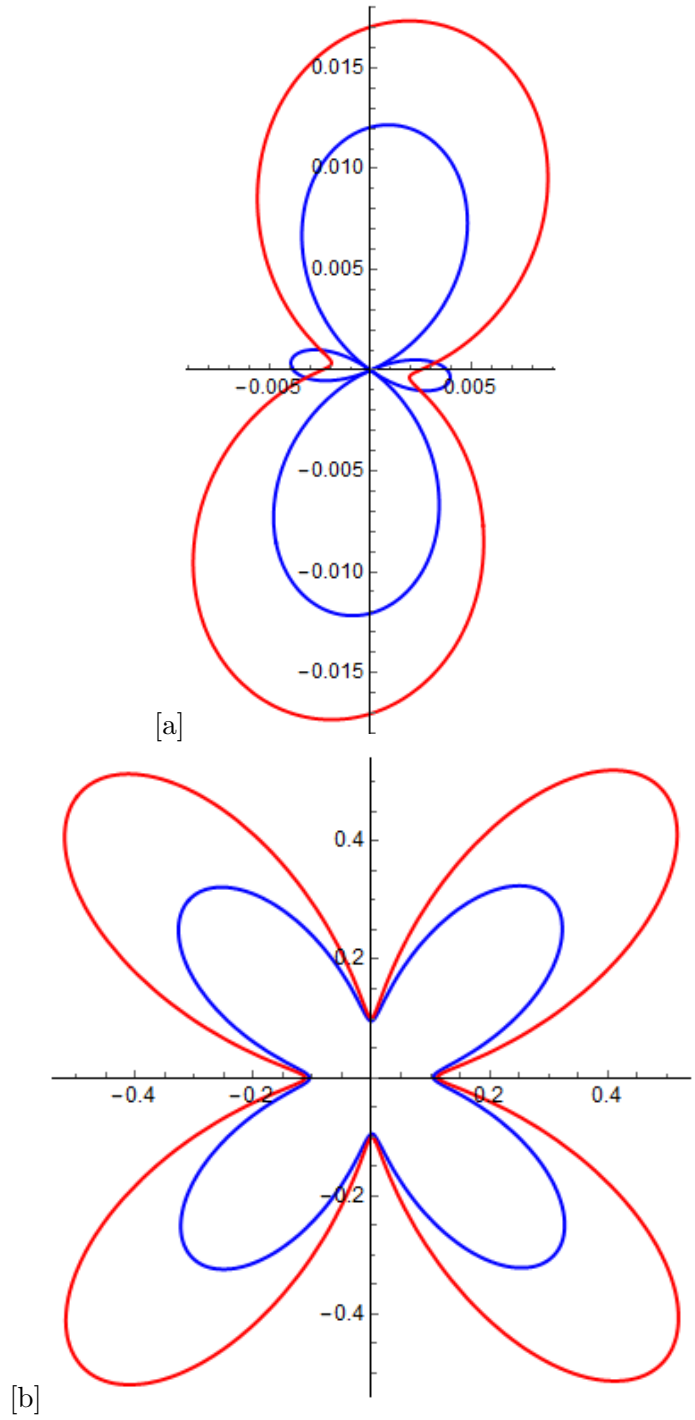

Figure 27: Variation of gradient with ϕ (for different cases of fracture weaknesses) for different wave modes. a)$G_{PP}(\phi)$ b) $G_{S_V-S_V}(\phi)$.

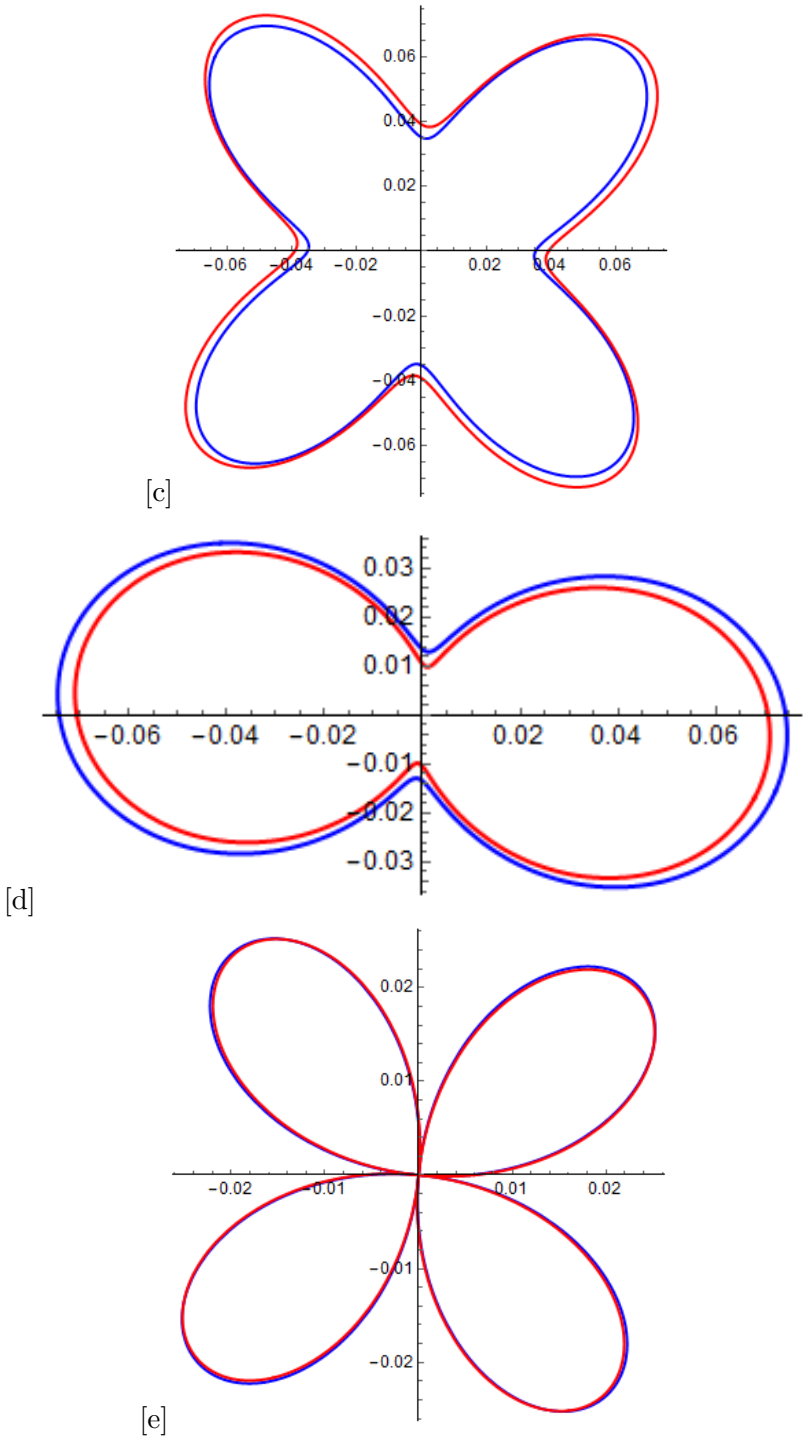

Figure 27: Variation of gradient with ϕ (for different cases of fracture weaknesses) for different wave modes. c)$G_{S_H-S_H}(\phi)$ d)$G_{P-S_V}(\phi)$ e)$G_{P-S_H}(\phi)$.

7 Monoclinic models from well log data

The well log parameters used to select VTI background medium are shown in figure 28. The medium obtained by upscaling of well log data is then permeated by two vertical fracture sets non-orthogonal to each other. Then the equivalent medium is monoclinic with a horizontal symmetry plane. Different sets of fracture weaknesses values and azimuth angles of fracture sets are provided in Appendix H.

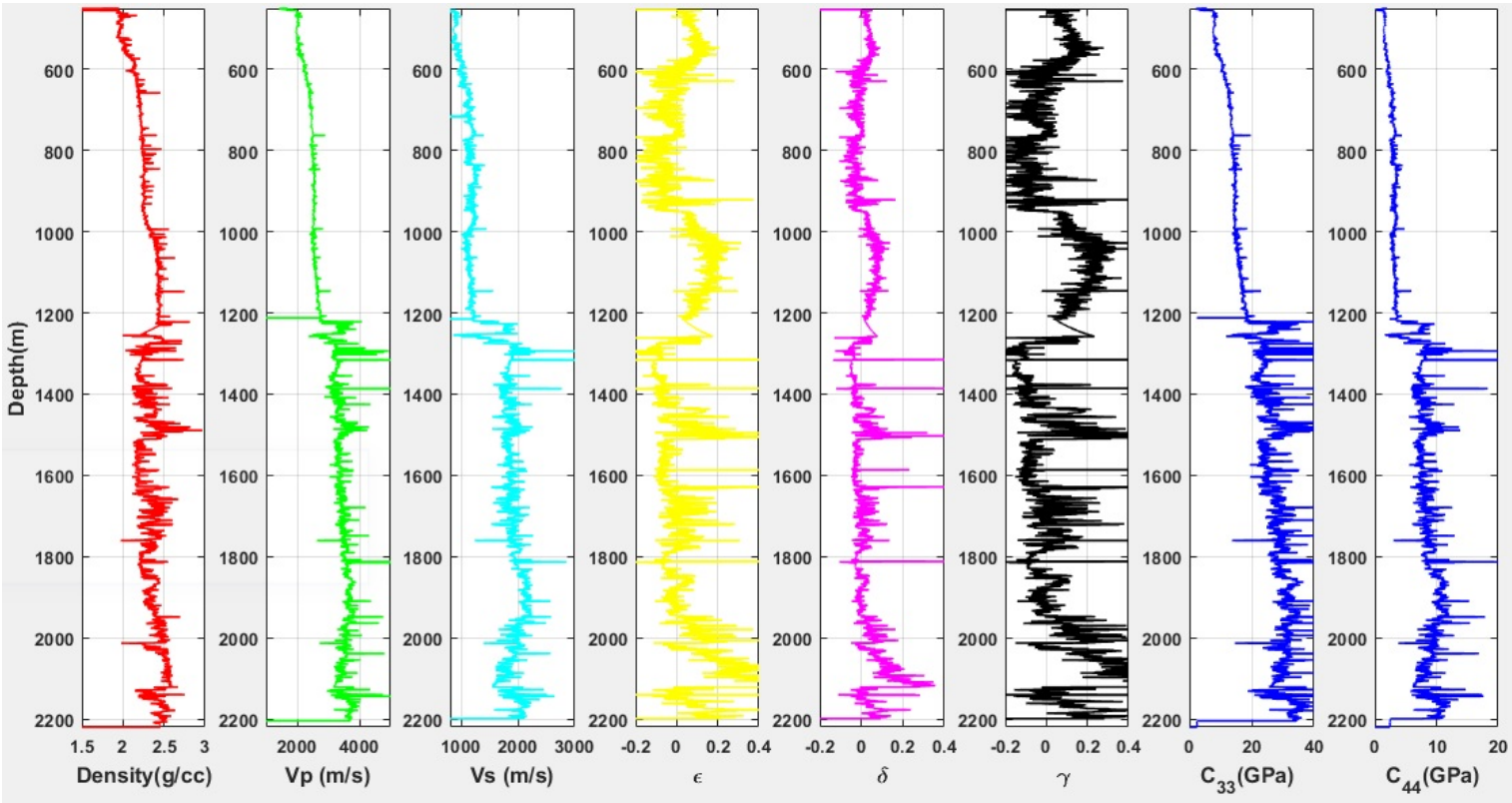

Figure 28: Plot of well log data with depth

The figure consists of plot of density, P- wave velocity, S- wave velocity, Thomsen anisotropic parameters (Thomsen, 1986) ϵ , δ, γ ,and stiffness coefficients C_{33} and C_{44}, respectively from left to right vs depth. Two zones showing strong variation in these properties, especially anisotropic parameters are selected for modeling using Backus averaging technique, to convert each zone to effective homogeneous media. The elastic properties of the effective medium depend on the degree of the vertical heterogeneity (Berryman et al., 1999) and the length of averaging (Sams and Williamson, 1994; Liner and Fei, 2006). The length of the averaging (zone considered) should be long enough so that properties of the medium are nearly independent in the vertical direction after smoothing . Since the rocks selected for modeling are buried at greater depths, it can

be noticed that the background stiffness values are also quite higher compared to the standard VTI bakground model (Schoenberg and Helbig, 1997).

Model	Depth of the zone		Density normalized effective stiffness coefficients-VTI background (GPa)					Density (g/cc)
	From(m)	To(m)	C_{33b}	C_{44b}	C_{11b}	C_{13b}	C_{66b}	
Model 1	1498.09	1515.01	11.36	3.32	14.48	5.29	4.52	2.38
Model 2	2006.04	2022.96	12.13	3.69	13.89	5	4.42	2.37

Table 1: Details of the zones from well log data for modeling.

7.1 Model 1

The details of the effective properties of VTI background medium for model 1 has been shown in table 1. The values of Thomsen anisotropic parameters ϵ , δ and γ for effective medium are 0.137, 0.052 and 0.18 respectively. These values suggest that the medium is weakly anisotropic and has characteristics similar to that of shale rock. Also, shear wave splitting could be significant in this model. The values for vertical propagation velocity for P and S waves are 3.37km/s and 1.82km/s respectively.

7.2 Model 2

The zone considered for Model 2 lies at greater depth than the zone for model 1. The values for vertical propagation velocity for P and S waves are 3.48km/s and 1.92km/s respectively and are higher than those for model 1, which is quite obvious. However, density of this effective medium is slightly lower than that of model 1. The values of Thomsen anisotropic parameters ϵ , δ and γ for effective background medium for model 2 are 0.072, 0.021 and 0.10 respectively. These values are quite low as compared to those for model 1, suggesting less anisotropic nature of the effective medium. This means anisotropic effects for various individual layers in this model are cancelling each other.

7.3 Description of study

The primary goal has been determining the orientation of fracture sets from seismic data, using inverse modeling technique and calculate the errors in azimuth angles so obtained. The details are provided in Appendix H. The NMO group ellipses of monoclinic models are analyzed with respect to the Thomsen anisotropic parameters of VTI background medium and it is observed that NMO group velocity coefficient A_{11} (responsible for rotation of NMO group ellipses) for P wave depends mainly on anisotropic parameters ϵ and γ. This coefficient for S waves depends mainly on anisotropic parameters ϵ and δ (Appendix I).

8 Discussion

8.1 Comparison of sensitivities

NMO velocity ellipses and AVAz gradients sensitivities toward fracture weaknesses in the case of VFTI media

Based on the data in the section 3.4 of report, the numerical values for sensitivities are calculated from both attributes. It was quite convenient to use the NMO velocities ellipse data to find out the sensitivities towards fracture weaknesses. This is due to straightforward nature of the expressions. AVAz gradient data set for orthorhombic or other highly anisotropic media are slightly complex. That's why two sets of fracture weaknesses were considered to observe the change in the curve of gradient vs azimuth angle ϕ. Comparison of sensitivities obtained from NMO velocities vs AVAz gradient attributes are shown in tables below:

Wave modes	j=1,2	$\tilde{A_{\delta_N,j}}$	$\tilde{A_{\delta_V,j}}$	$\tilde{A_{\delta_H,j}}$
PP	j=1	-0.68	-1.28	0
	j=2	-0.21	0	0
S_1S_1	j=1	-1.05	1.42	0
	j=2	0	0	-1.0
S_2S_2	j=1	0	0	-1.0
	j=2	-0.03	0	0
PS_1	j=1	-0.87	0.07	0
	j=2	-0.1	0	-0.5
PS_2	j=1	-0.34	-0.64	-0.50
	j=2	-0.12	0	0
S_1S_2	j=1	-0.52	0.71	-0.50
	j=2	-0.01	0	-0.50

Table 2: Sensitivities toward fracture weaknesses from NMO Velocities ellipse data set.

Wave modes	j j=1,2,3	coefficients of fracture weaknesses $\tilde{A_{\delta_N,j}}$	$\tilde{A_{\delta_V,j}}$	$\tilde{A_{\delta_H,j}}$
PP	j=1	-6.97	13.25	0
	j=2	-1.72	0	0
$S_V S_V$	j=1	0.7	0.5	0
	j=2	0.4	1	0
	j=3	-0.25	0	0.25
$S_H S_H$	j=1	0	0	0.25
	j=2	0.08	0	-0.4
PS_V	j=1	-0.06	0.26	0
PS_H	j=2	0.06	-0.26	0
$S_V S_H$	j=1,2	0	0	0

Table 3: Sensitivities toward fracture weaknesses from AVAz gradient attribute.

NMO group velocity ellipses sensitivities toward fractures in the case of monoclinic media

Here, I tried to analyze how the group velocity coefficients of NMO group ellipses for P, S_1 and S_2 wave modes vary with both the magnitude of fracture weaknesses and orientations of fracture systems. Several different azimuth angles of fracture sets were considered and corresponding change in group velocity coefficients were noticed. Two different cases for fracture weaknesses of fracture sets were considered. In first case, the fracture weaknesses of both fracture sets are identical and in the second case, the fracture weaknesses of one fracture set are different than the fracture weaknesses of other set. The details are provided in table no. 4 and 5. It was found that the changes are significant for shear waves. The following tables are based on the VTI backgound standard model typical for sedimentary rocks like shale (Schoenberg and Helbig, 1997).

Fracture weaknesses	$\delta_{N1} = \delta_{N2} = 0.1$,$\delta_{V1} = \delta_{V2} = 0.2$,$\delta_{H1} = \delta_{H2} = 0.3$			
Fracture sets orientation	Wave modes	A_{20}	A_{11}	A_{02}
$\phi_1 = 0°$, $\phi_2 = 0°$	P	0.23	0	0.15
	S_1	0.13	0	0.53
	S_2	0.53	0	0.2
$\phi_1 = 20°$, $\phi_2 = -15°$	P	0.22	-0.0002	0.155
	S_1	0.23	-0.0005	0.47
	S_2	0.47	-0.0007	0.29
$\phi_1 = 30°$, $\phi_2 = -20°$	P	0.22	-0.0004	0.16
	S_1	0.31	-0.02	0.42
	S_2	0.42	0.018	0.35
$\phi_1 = 45°$, $\phi_2 = -30°$	P	0.2	-0.0002	0.18
	S_1	0.41	-0.025	0.36
	S_2	0.36	0.024	0.43
$\phi_1 = 60°$, $\phi_2 = -45°$	P	0.18	0.0002	0.2
	S_1	0.43	0.03	0.36
	S_2	0.36	-0.03	0.41
$\phi_1 = 60°$, $\phi_2 = -60°$	P	0.17	0	0.21
	S_1	0.4	0	0.39
	S_2	0.39	0	0.36
$\phi_1 = 90°$, $\phi_2 = -90°$	P	0.15	0	0.23
	S_1	0.2	0	0.53
	S_2	0.53	0	0.13

Table 4: Group velocity coefficients when both fracture sets have identical fracture weaknesses.

Fracture weaknesses	$\delta_{N1} = 0.1, \delta_{N2} = 0.15, \delta_{V1} = 0.2, \delta_{V2} = 0.2, \delta_{H1} = 0.3, \delta_{H2} = 0.35$			
Fracture sets orientation	Wave modes	A_{20}	A_{11}	A_{02}
$\phi_1 = 0°$, $\phi_2 = 0°$	P	0.24	0	0.15
	S_1	0.14	0	0.55
	S_2	0.55	0	0.2
$\phi_1 = 20°$, $\phi_2 = -15°$	P	0.23	0.0002	0.16
	S_1	0.25	-0.0064	0.48
	S_2	0.48	0.0073	0.3
$\phi_1 = 30°$, $\phi_2 = -20°$	P	0.22	0.0002	0.165
	S_1	0.33	-0.0258	0.43
	S_2	0.43	0.0266	0.37
$\phi_1 = 45°$, $\phi_2 = -30°$	P	0.2	0.0005	0.18
	S_1	0.43	-0.0274	0.37
	S_2	0.37	0.03	0.45
$\phi_1 = 60°$, $\phi_2 = -45°$	P	0.18	0.0011	0.2
	S_1	0.46	0.03	0.36
	S_2	0.36	-0.025	0.44
$\phi_1 = 60°$, $\phi_2 = -60°$	P	0.17	0.0007	0.22
	S_1	0.42	-0.003	0.39
	S_2	0.39	0.007	0.39
$\phi_1 = 90°$, $\phi_2 = -90°$	P	0.15	0	0.24
	S_1	0.2	0	0.55
	S_2	0.55	0	0.14

Table 5: Group velocity coefficients when fracture sets have non-identical fracture weaknesses.

8.2 Error analysis

Two main type of error has been encountered in determining the orientation of fracture sets from the seismic data. One is inherent to inverse modeling using NMO group-velocity ellipses. And the other comes from inaccurate measurement of fracture weaknesses. The magnitude of error depends on the background VTI model and wave modes selected for calculations .

8.2.1 Related to Inverse modeling

Group velocity coefficient A_{11} of NMO group ellipses are utilized for inverse modeling. This is because other group velocity coefficients fail to give satisfactory estimate of azimuth angles of fracture sets and often give multiple solutions.
Let ϕ_i be azimuth angle of fracture sets fixed for forward modeling
$\phi_i^{'}$ is fracture sets orientation as calculated from group velocity coefficients, with $i = 1, 2$

then
$\Delta\phi_i = \mid \phi_i^{'} \mid - \mid \phi_i \mid$=Error in orientation of fracture sets.
Case 1: The fracture weaknesses of both fracture sets are identical,
$\delta_{N1} = \delta_{N2} = 0.1$
$\delta_{V1} = \delta_{V2} = 0.2$
$\delta_{H1} = \delta_{H2} = 0.3$
Case 2: The fracture weaknesses of fracture sets are non-identical,
$\delta_{N1} = 0.1, \delta_{N2} = 0.15$
$\delta_{V1} = 0.2, \delta_{V2} = 0.2$
$\delta_{H1} = 0.3, \delta_{H2} = 0.35$
The colour 'cyan' in the cells of table indicate that calculations done using wave modes S_1 and S_2 give good estimate of fracture sets orientation. Cell colour 'pink' means wave modes P, S_1 or P, S_2 are giving less error values. This table is based on the standard VTI background model.

Fracture weaknesses	Identical for both fracture sets			Different for fracture sets	
Actual azimuth angles (fracture orientation)	Wave modes considered	Error (°)		Error (°)	
		$\Delta\phi_1$	$\Delta\phi_2$	$\Delta\phi_1$	$\Delta\phi_2$
$\phi_1 = 20°$, $\phi_2 = -15°$	P, S_1	-0.38	-0.47	-0.14	-0.16
	P, S_2	-0.54	-0.33	-0.22	-0.11
	S_1, S_2	-0.04	-0.01	0.01	0.02
$\phi_1 = 30°$, $\phi_2 = -20°$	P, S_1	-0.32	0.7	0.27	-0.6
	P, S_2	-0.32	0.7	0.17	-0.58
	S_1, S_2	-0.32	0.67	-0.06	0.17
$\phi_1 = 45°$, $\phi_2 = -30°$	P, S_1	-0.25	-1.05	-3.2	0.4
	P, S_2	-0.25	-1.1	-2.97	0.34
	S_1, S_2	-0.1	-1.01	-76.5	3.03
$\phi_1 = 60°$, $\phi_2 = -45°$	P, S_1	-0.13	-0.73	1.6	3.89
	P, S_2	-0.2	-0.75	-41.1	6.56
	S_1, S_2	1.05	0.5	-38.5	7.43
$\phi_1 = 60°$, $\phi_2 = -60°$	P, S_1	Non-	Non-	1.7	-1.36
	P, S_2	Unique	Unique	0.9	-1.3
	S_1, S_2	solutions	solutions	73.8	-68.9

Table 6: Error in estimation of azimuth angles using Group velocity coefficient A_{11}.

8.2.2 Related to Error in fracture weaknesses measurement

Let $(\phi_f)_i$ be fracture sets orientation calculated using accurate fracture weaknesses $(\phi_{fE})_i$ is fracture sets orientation calculated using wrongly measured fracture weaknesses, with $i = 1, 2$ then
$\Delta\phi_{Ei} = (\phi_f)_i - (\phi_{fE})_i$ =Error in orientation of fracture sets.

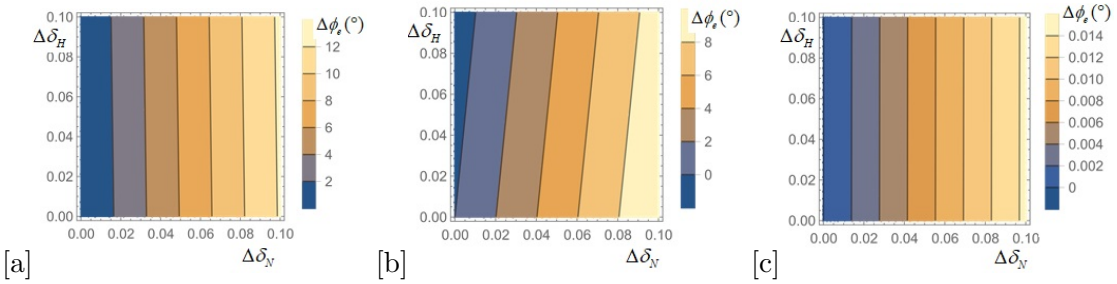

Figure 29: Variation of error in azimuth angle with error in fracture weaknesses measurements.The azimuth angles are calculated utilizing parameters from NMO ellipse for wave modes a) P, S_1 b) P, S_2 c) S_1, S_2

But to see the continuous variation of error, we need to find the derivative of azimuth angle calculated from inverse modeling which is a function of background stiffnesses, group velocity coefficients and fracture weaknesses. This expression has the following general form: $\phi^{'} = (f_1.\delta_N)^{'} + (f_2.\delta_H)^{'}$ where $f_{1,2} = f(c_{ijb}, [A_{11}]_{P,S_1,S_2})$

8.3 Comparison of study from different monoclinic models

Three monoclinic models were considered in this study. These models differ primarily in their VTI background medium. One is based on a standard model typical of shale (Schoenberg and Helbig, 1997). Two others namely model 1 and model 2 have their VTI background medium derived from upscaling of well log data at different intervals. It can be mentioned that any seismic attributes, normal move-out velocities ellipse or amplitude vs azimuth's gradient depends strongly on the background stiffness coefficients and fracture parameters. I would like to stress here on error in azimuth angle calculation from NMO group ellipses data. For all the models, S_1 and S_2 wave modes are best choice for determining orientations of fracture sets. The error in this estimate seems to be dependent on the magnitude of anisotropy for the host rock. Higher it is, more is the error (In this case, it is highest for standard model, then model 1 and least for model 2). But this error also depend on wave modes considered, say in model 1, inverse modeling from group velocity coefficients A_{11} for P and S_1 waves gives less error in azimuth angle estimate for respective coefficients in model 2.

There also exist certain similarities in the conclusions drawn from analysis of all these models. Firstly, the shear wave are more sensitive to fractures than P-wave. Secondly, amplitude vs azimuth's gradient in the reflection coefficient for PP wave mode is significantly sensitive to fracture in all of these models. The pattern in the variation of NMO group ellipses with orientation of fracture systems are also quite similar. And all the sensitivity analyses done on NMO velocities and AVAz gradients for different wave modes in the case of standard model equally hold for model 1 and model 2.

8.4 Future Works

For simplicity, the fractures were considered long and thin. There is a need to understand the impact of fracture filling materials on these attributes, i.e. on normal-moveout velocities (NMO ellipses) and amplitude vs azimuth (AVAz) data for P, S_1 and S_2 wave modes. Geologically, fractures may not be evenly spaced throughout the large region or it may even form a cluster. It is therefore, important to study these effects in terms of fracture density. Also in most of the cases, fracturing in rocks are considered vertical but there are several cases where fracture surface can be tilted. These are some of the scenario that should be analyzed in continuity to the current work.

9 Conclusion

The conclusions made on the basis of fracture characterization from two attributes, NMO velocities ellipse and AVAz gradient are summarized here.
In the case of VFTI media, the eccentricity of NMO velocity ellipse for PP wave mode depends on both normal and vertical tangential fracture weaknesses, i.e. δ_N and δ_V but sensitivity towards δ_V is much higher. Similar analyses were done for other pure wave modes and converted PS_1, PS_2 and S_1S_2 wave modes using this approach. NMO velocity ellipse's eccentricity for converted wave modes PS_2 and S_1S_2 are found to be sensitive to all fracture weaknesses, i.e. δ_N, δ_V and δ_H . For monoclinic media, NMO velocity ellipses for shear waves are more sensitive to fracture as compared to that of P -wave. NMO group velocity coefficient A_{11}, responsible for rotation of NMO group ellipses for S_1 and S_2 wave modes is best choice for inverse modeling. This is because the orientation of systems of fracture based on calculated azimuth angles from equations for group velocity coefficient A_{11} for S_1 and S_2 waves are quite closer to the actual orientation of the fracture sets. Although, there is a limitation in the application of this parameter for inverse modeling. The actual angle between strike of two fracture sets should neither be too less (closer to 0 degree), nor too high (90 degrees). At those extreme angles, the effective medium turns to be orthorhombic. The error in azimuth angle estimation due to wrong measurements of fracture weakness values is mainly sensitive to error in δ_N.

Sensitivity towards fracture are much higher for amplitude vs azimuth (AVAz) gradient data compared to NMO velocities data. Reflection amplitudes have advantages over seismic velocities and thereby having higher vertical resolution. Even for PP- wave mode, gradient term in the reflection coefficient of AVAz data is sensitive to fracture. Significant effect could be observed in the reflection coefficients for different wave modes with small changes in fracture systems, both in terms of orientation and magnitude of fracture weaknesses. However, using NMO velocities data for fractured media, one gets more comprehensive information than AVAz attribute. This means NMO ellipse data can be easily applied for inversion to fracture parameters. While working with amplitude vs azimuth, apart from gradient terms in reflection coefficients, we need to consider curvature terms as well for such inversion. The overall equation has higher orders of trigonometric functions of azimuth angles and can be complicated.

Finally, I performed a cross-check of the theory with the computation of NMO group velocity ellipses and azimuth angles of fracture systems for two monoclinic models. Firstly, upscaling of well log data was done to get VTI background medium, which was then permeated by two non-orthogonal vertical fracture sets. Furthermore, analysis of error in orientation estimate from inverse modeling was carried out. I obtained results that are similar to the ones for standard model. So, it can be agreed upon the fact that conclusions made are applicable, in general for any fractured rock having transversely isotropic background with vertical axis of symmetry.

ACKNOWLEDGMENTS

I am grateful to my supervisor Alexey Stovas for his guidance, patience and support throughout this work. He regularly helped me to improve my knowledge and understanding of the subject. I am thankful to Jin Song (PhD, IGP, NTNU) for sharing his ideas, providing necessary materials and his concern towards the progress of my work. I would also like to thank other members of our Friday seminar group. Seminars were very resourceful. Within a short span of time, I learned about a lot of topics related to seismic anisotropy. Most importantly, I developed critical thinking, presentation and questioning skills.

This semester was a bit special with Corona virus forcing us several times to carry out activities digitally. However thanks to the combined effort of our group, I was able to continue the work without too much difficulty.

References

Anderson, D. L. , 1962. *Elastic Wave Propagation in Layered Anisotropic Media*, Journal of Geophysical research, Vol. 66, No. 9 .

Aki, K., and P. G. Richards, 1980 *Quantitative seismology: Theory and methods*, W. H. Freeman Co.

Backus, G. E. , 1962. *Long-Wave Elastic Anisotropy Produced by Horizontal Layering*, Journal of Geophysical research, Vol. 67, No. 11 .

Bagheri, M. and Settari, A. , 2008. *Modeling Coupled Fluid Flow and Deformation of Fractured Reservoirs Using Full Tensor Permeability*, Paper presented at the Europec/EAGE Conference and Exhibition, Rome, Italy.

Bakulin, A., Grechka, V., and I. Tsvankin , 2000. *Estimation of fracture parameters from reflection seismic data—Part III: Fractured models with monoclinic symmetry*, Geophysics 65, 1818-1830 .

Barenblatt, G.I., Zheltov, Iu.P., and Kochina, I.N. , 1960. *Basic concepts in the theory of seepage of homogeneous liquids in fissured rocks*, J. Appl. Math. Mech., 24, pp. 1286–1303.

Berryman, J. G., Grechka, V. Y., and Berge, P. A, , 1999. *Analysis of Thomsen parameters for finely layered VTI media*, Geophysical Prospecting, 47, 959 – 978 .

Carcione J. M. , Santos J.E. , Picotti, S. , 2012. *Fracture-Induced Anisotropic Attenuation*, Rock Mech Rock Eng DOI 10.1007/s00603-012-0237-y .

Fan L.F., Ren F., Ma G.W. , 2011. *An extended displacement discontinuity method for analysis of stress wave propagation in viscoelastic rock mass.*, J Rock Mech Geotech Eng 3:73-81 .

Farra, V., Psencik, I., and P. Jilek , 2016. *Weak-anisotropy moveout approximations for P waves in homogenous layers of monoclinic or higher anisotropy symmetries.*, Geophysics 81, no.2, C17-C37 .

Grechka, V. and Kachanov, M., 2006. *Seismic characterization of multiple fracture sets: Does orthotropy suffice?*, Geophysics, Vol. 71, No. 3 ; P. D93–D105.

Grechka, V., Tsvankin I. and J.K. Cohen, 1999. *Generalized Dix equation and analytic treatment of normal-moveout velocity for anisotropic media*, Geophysical Prospecting 47, 117-148.

Hood, J. A., and Schoenberg, M., 1989. *Estimation of vertical fracturing from measured elastic moduli*, J. Geophys. Res., 94, 15611-15618.

Hudson J.A., 1980 *Overall properties of a cracked solid*, Mathematical Proceedings of the Cambridge Philosophical Society 88, 371-384

Jaeger, J. C., 1969. *Elasticity, fracture and flow, with engineering and geological applications, 3d ed.*, London, Chapman and Hall, 268 p.

Jin, S. & Stovas, A., 2020. *Exact and approximate reflection/transmission responses from a layer containing vertical fractures*, Geophys. J. Int., 222, 260–288

Jin, S. & Stovas, A., 2020. *Reflection and transmission approximations for monoclinic media with a horizontal symmetry plane*, Geophysics, Vol. 85 No. 1 , P. C13–C36

Jones, J. P., and J. S. Whittier, 1967. *Waves at a flexibly bonded interface*, Journal of Applied Mechanics, 34, 905–909, doi: 10.1115/1.3607854.

Kachanov, M. , 1980. *Continuum Model of Medium with Cracks*, Journal of the Engineering Mechanics Division, 1980, Vol. 106, Issue 5, Pg. 1039-1051

Leviant, V., Petrov, I. and Kvasov I., 2019. *Numerical Modeling of Seismic Responses from Fractured Reservoirs by the Grid-characteristic Method*, Geophysical Developments Series No. 17, Society of Exploration Geophysicists, ISBN 978-0-931830-41-9

Liner, C. L., and Fei T. W., 2006. *Waves at a flexibly bonded interfaceLayer-induced seismic anisotropy from full-wave sonic logs: theory, applications, and validation*, Geophysics, 71, d183-D190

Mehdi E. Far, 2011. *Seismic Characterization of Naturally Fractured Reservoirs*, Dissertation, Department of Earth and Atmospheric Sciences University of Houston

Mohaghegh S.d., 2017. *A textbook on Shale analytics-Data-driven analytics in unconventional resources*, Springer International, ISBN 978-3-319-48753-3 (eBook) DOI 10.1007/978-3-319-48753-3

Nichols, D., Muir, F., and Schoenberg, M., 1989. *Elastic properties of rocks with multiple sets of fractures*, Soc. Expl. Geophys., Expanded Abstracts, 471-474.

Perino A., Zhu, J.B., Li J.C., Barla G., Zhao J., 2010. *Theoretical methods for wave propagation across jointed rock masses.*, Rock Mech Rock Eng 43:799–809

Priest, S. D., and J. A. Hudson., 1976. *Discontinuity spacings in rock*, International Journal of Rock Mechanics Mining Sciences and Geomechanics Abstracts, v. 13, p. 135–148.

Pyrak-Nolte L.J., Myer L.R., Cook N.G.W., 1990. *Transmission of seismic waves across single natural fractures.*, J Geophys Res 95:8617–8638

Rytov, S.M. , 1956. *Electromagnetic Properties of a Finely Stratified Medium*, J. Exper. Theoret. Phys. USSR, Vol. 2, No. 3;29, 605-616 .

Sams, M. S., and Williamson, P. R., 1994. *Backus averaging, Scattering and drift*, Geophysical prospecting, 42, 541-564.

Schoenberg, M., 1980. *Elastic wave behavior across linear slip interfaces*, Journal of the Acoustical Society of America, 68, 1516–1521, doi: 10.1121/1.385077.

Schoenberg,M. & Sayers, C.M., 1995. *Seismic anisotropy of fractured rock*, Geophysics, 60(1), 204–211.

Schoenberg, M. & Helbig, K., 1997. *Orthorhombic media: modeling elastic wave behavior in a vertically fractured earth*, Geophysics, 62(6), 1954–1974.

Schultz, R.A., and Fossen, H., 2008. *Terminology for structural discontinuities*, American Association of Petroleum Geologists Bulletin 92, 853–867.

Stovas, A. & Hao, Q., 2015. *Lecture notes on the course TPG-4125 Seismic wave propagation*, Norwegian University of Science and Technology, Trondheim.

Stovas, A., 2021. *On parameterization in monoclinic media with a horizontal symmetry plane*, Geophysics, Vol. 86 No. 1 , P. C37–C49

Stovas, A. and Ursin, B., 2003. *Reflection and transmission responses of layered transversely isotropic viscoelastic media*, Geophysical Prospecting, 51, 447–477, doi: 10.1046/j.1365-2478.2003.00381.x.

Stovas, A. and Arntsen, B., 2006. *Vertical propagation of low – frequency waves in finely layered media*, Geophysics, 71, T87 – T94.

Thomsen, L., 1986. *Weak elastic anisotropy*, Geophysics, 51, 1954–1966.

Torsæter, O., 2018. *Lecture notes on Fractured reservoirs*, Norwegian University of Science and Technology, NTNU Trondheim.

Tsvankin, I., 1997. *Reflection moveout and parameter estimation for horizontal transverse isotropy*, Geophysics, 62, 614-629.

Twiss R.J. and Moores E.M., 1992. *Structural geology*, W.H. Freeman Company, New York. 532p.

Worthington, M. H., 2008. *Interpreting seismic anisotropy in fractured reservoirs*, First Break, 26, 57–63.

Yu-Shu Wu, 2016. *Multiphase Fluid Flow in Porous and Fractured Reservoirs*, Elsevier Inc.,ISBN 978-0-12-803848-2

Appendix

A: Stiffness Coefficients for Equivalent ORT Media

For an orthorhombic medium, the stress-strain relationship has the matrix form

$$\begin{bmatrix}\sigma_1\\ \sigma_2\\ \sigma_3\\ \sigma_4\\ \sigma_5\\ \sigma_6\end{bmatrix} = \rho \begin{bmatrix} c_{11} & c_{12} & c_{13} & 0 & 0 & 0\\ c_{12} & c_{22} & c_{23} & 0 & 0 & 0\\ c_{13} & c_{23} & c_{33_b} & 0 & 0 & 0\\ 0 & 0 & 0 & c_{44_b} & 0 & 0\\ 0 & 0 & 0 & 0 & c_{55} & 0\\ 0 & 0 & 0 & 0 & 0 & c_{66}\end{bmatrix} \begin{bmatrix}\epsilon_1\\ \epsilon_2\\ \epsilon_3\\ \epsilon_4\\ \epsilon_5\\ \epsilon_6\end{bmatrix} \tag{A.1}$$

VTI background 6 x 6 stiffness matrix can be written as :

$$C_b = \begin{bmatrix} c_{11_b} & c_{12_b} & c_{13_b} & 0 & 0 & 0\\ c_{12_b} & c_{11_b} & c_{13_b} & 0 & 0 & 0\\ c_{13_b} & c_{13_b} & c_{33_b} & 0 & 0 & 0\\ 0 & 0 & 0 & c_{44_b} & 0 & 0\\ 0 & 0 & 0 & 0 & c_{44_b} & 0\\ 0 & 0 & 0 & 0 & 0 & c_{66_b}\end{bmatrix} \tag{A.2}$$

The fracture compliance 3 x 3 matrix:

$$Z = \begin{bmatrix} Z_N & 0 & 0\\ 0 & Z_V & 0\\ 0 & 0 & Z_H\end{bmatrix} \tag{A.3}$$

The change Δ in the compliance matrix attributable to the introduction of an orthotropic fracture set perpendicular to the x_1-axis [see the last equation of Nichols et al. (1989)] is

$$\Delta = \begin{bmatrix} Z_N & 0 & 0 & 0 & 0 & 0\\ 0 & 0 & 0 & 0 & 0 & 0\\ 0 & 0 & 0 & 0 & 0 & 0\\ 0 & 0 & 0 & 0 & 0 & 0\\ 0 & 0 & 0 & 0 & Z_V & 0\\ 0 & 0 & 0 & 0 & 0 & Z_H\end{bmatrix} \tag{A.4}$$

Hence, the compliance matrix of the medium equivalent, in the long-wavelength limit, to the VFTI medium is $(\rho C_b)^{-1} + \Delta$, and its density-normalized stiffness matrix is given by

$$C_e = [C_b)^{-1} + \rho\Delta]^{-1} = C_b[I + \rho\Delta C_b]^{-1} \tag{A.5}$$

For simplification of the resulting stiffness matrix, dimensionless quantities are defined as

$$0 \le \delta_N \equiv \frac{Z_N \rho c_{11_b}}{1 + Z_N \rho c_{11_b}} < 1, 0 \le \delta_V \equiv \frac{Z_V \rho c_{44_b}}{1 + Z_N \rho c_{44_b}} < 1, 0 \le \delta_H \equiv \frac{Z_H \rho c_{66_b}}{1 + Z_N \rho c_{66_b}} < 1, \tag{A.6}$$

Where c_{11_b}, $c_{44_b}$and c_{66_b} are positive (Schoenberg and Helbig, 1997). These are termed as fracture weaknesses.

The density-normalized stiffness matrix of the equivalent medium is given by

$$C_e = \begin{bmatrix} c_{11_b}(1-\delta_N) & c_{12_b}(1-\delta_N) & c_{13_b}(1-\delta_N) & 0 & 0 & 0 \\ & c_{11_b}(1-\delta_N\frac{c_{12_b}^2}{c_{11_b}^2}) & c_{13_b}(1-\delta_N\frac{c_{12_b}}{c_{11_b}}) & 0 & 0 & 0 \\ & & c_{33_b}(1-\delta_N\frac{c_{13_b}^2}{c_{11_b}c_{33_b}}) & 0 & 0 & 0 \\ & & & c_{44_b} & 0 & 0 \\ & & & & c_{44_b}(1-\delta_V) & 0 \\ & & & & & c_{66_b}(1-\delta_H) \end{bmatrix} \tag{A.7}$$

B: Slowness surface of VFTI media

Substituting a plane-wave displacement of the form

$$\boldsymbol{u}expi\omega(s.x-t) \tag{B.1}$$

, where s is the slowness vector and $\boldsymbol{u}$ is the unit displacement polarization vector, and the general anisotropic stress-strain relationship

$$\sigma_{ij} = \rho c_{ijkl}\epsilon_{kl} \tag{B.2}$$

into the equations of motion for an elastic medium gives the Christoffel equation (Schoenberg and Helbig, 1997),

$$[\Gamma_{jk}(s_1,s_2,s_3)-\delta_{jk}]u_k \equiv [c_{ijkl}s_is_l-\delta_{jk}]u_k = 0 \tag{B.3}$$

The slowness surface is made up of the end points of all vectors s that cause the determinant of the Christoffel equation to vanish, i.e., that satisfy

$$\mid \Gamma(s) - I \mid = 0 \tag{B.4}$$

, where I is the 3 x 3 identity matrix

When the medium is orthorhombic, this equation takes the following matrix form of the Christoffel equation for an orthorhombic medium.

$$\begin{bmatrix} c_{11}s_1^2+c_{66}s_2^2+c_{55}s_3^2-1 & (c_{12}+c_{66})s_1s_2 & (c_{13}+c_{55})s_1s_3 \\ (c_{12}+c_{66})s_1s_2 & c_{66}s_1^2+c_{22}s_2^2+c_{44}s_3^2-1 & (c_{23}+c_{44})s_2s_3 \\ (c_{13}+c_{55})s_1s_3 & (c_{23}+c_{44})s_2s_3 & c_{55}s_1^2+c_{44}s_2^2+c_{33}s_3^2-1 \end{bmatrix} \begin{bmatrix} u_1 \\ u_2 \\ u_3 \end{bmatrix} = \begin{bmatrix} 0 \\ 0 \\ 0 \end{bmatrix} \tag{B.5}$$

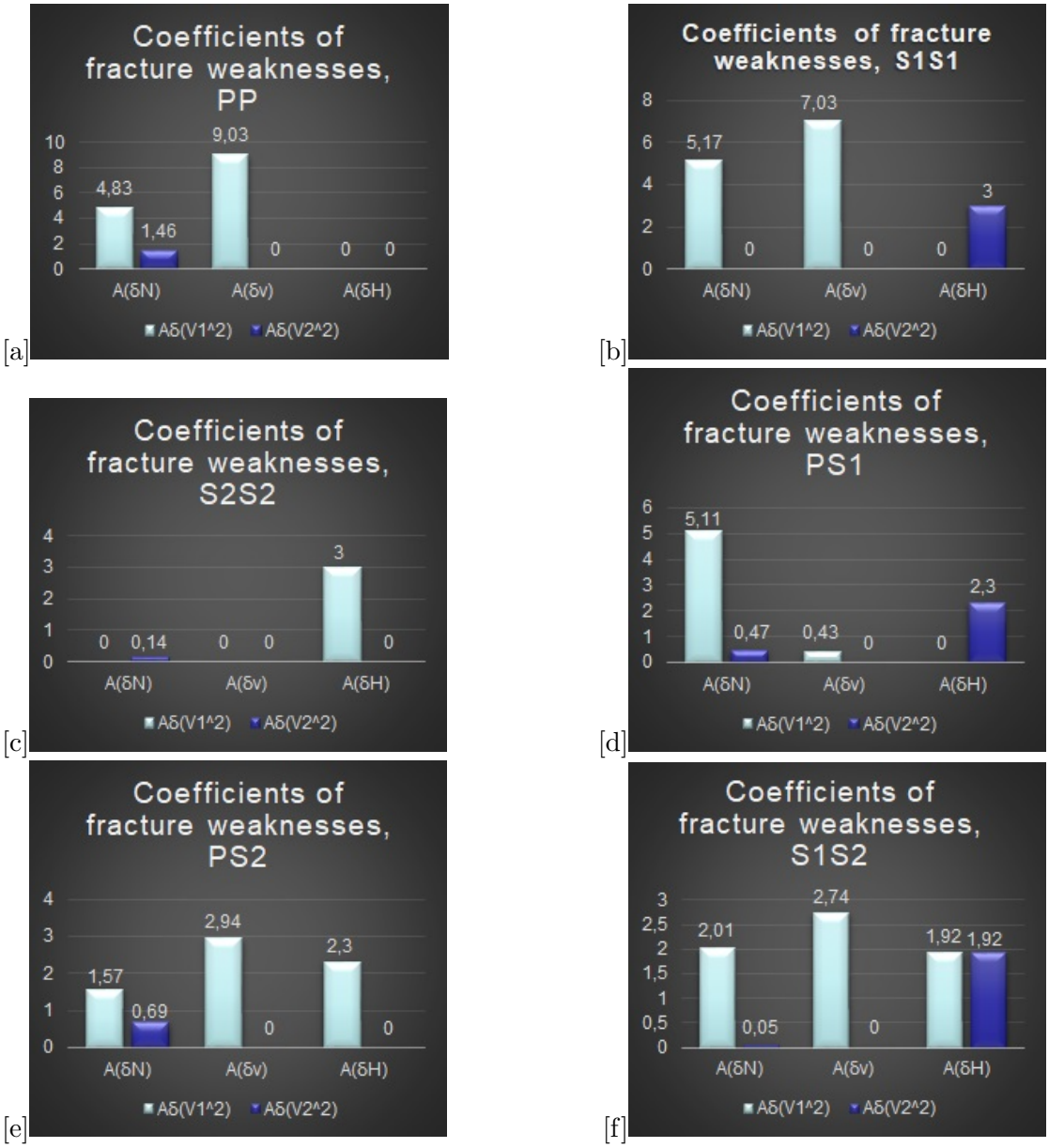

Figure 30: Squared NMO velocities sensitivities towards fracture weaknesses for VFTI media in XZ and YZ symmetry planes

C: Graphs for squared NMO velocities sensitivities towards fracture weaknesses

D: Contrast in isotropic Parameters and changes in Anisotropy Parameters

The Contrast in isotropic Parameters and changes in Anisotropy Parameters for the AVAz model of VFTI media can be given as (Song J. and Stovas A., 2020)

Contrast in isotropic Parameters:

$$\frac{\Delta Z_P}{\overline{Z}_P} = \frac{\Delta Z_P^{VTI}}{\overline{Z}_P^{VTI}} - \frac{(1-2g^2)^2}{2}\delta_N$$

$$\frac{\Delta V_P}{\overline{V}_P} = \frac{\Delta V_P^{VTI}}{\overline{V}_P^{VTI}} - \frac{(1-2g^2)^2}{2}\delta_N$$

$$\frac{\Delta V_S}{\overline{V}_S} = \frac{\Delta V_S^{VTI}}{\overline{V}_S^{VTI}} - \frac{1}{2}\delta_V$$

$$\frac{\Delta G_S}{\overline{G}_S} = \frac{\Delta G_S^{VTI}}{\overline{G}_S^{VTI}} - \delta_V$$

Where, $g = \frac{\overline{V}_S}{\overline{V}_P}$ is the ratio of average S wave velocity to average P wave velocity and $\delta_N, \delta_V \delta_H$ are fracture weaknesses.
$V_P^{VTI}, V_S^{VTI}, Z_P^{VTI}$ and G_S^{VTI} are the vertical P-wave velocity, vertical S-wave velocity, vertical P-wave impedance and vertical shear wave modulus for the VTI host medium.

changes in Anisotropy Parameters:

$$\Delta\epsilon_1 = 0$$
$$\Delta\epsilon_2 = 2g^2(g^2-1)\delta_N$$
$$\Delta\gamma_1 = \frac{1}{2}(\delta_V - \delta_H)$$
$$\Delta\gamma_3 = \frac{1}{2}\delta_V$$
$$\Delta\delta_1 = 0$$
$$\Delta\delta_2 = 2g^2[(2g^2-1)\delta_N - \delta_V]$$
$$\Delta\delta_3 = 2g^2[\delta_N - \delta_H]$$

Where, ϵ, γ and δ are Thomsen like parameters acting in different planes

E: Stiffness Coefficients for Effective monoclinic media

VTI background 6 x 6 stiffness matrix remains the same as given in equation A.2
The fracture compliance 6 x 6 matrix:

$$\Delta = \begin{bmatrix} K_N & 0 & 0 & 0 & 0 & 0 \\ 0 & 0 & 0 & 0 & 0 & 0 \\ 0 & 0 & 0 & 0 & 0 & 0 \\ 0 & 0 & 0 & 0 & 0 & 0 \\ 0 & 0 & 0 & 0 & K_V & 0 \\ 0 & 0 & 0 & 0 & 0 & K_H \end{bmatrix} \tag{E.1}$$

and the fracture compliances can be expressed in term of fracture weaknesses:

$$K_N = \frac{\delta_N}{c_{11_b}(1-\delta_N)}, K_V = \frac{\delta_V}{c_{44_b}(1-\delta_V)}, K_H = \frac{\delta_H}{c_{66_b}(1-\delta_H)} \tag{E.2}$$

Where c_{11_b}, $c_{44_b}$and c_{66_b} are positive.
Let ϕ_1 and ϕ_2 be the azimuth angle of fracture set 1 and fracture set 2 respectively. Then rotated fracture compliance matrix is given by $R(\phi_n)\Delta R^T(\phi_n)$, where n = 1,2.
And the Bond matrix for azimuthal rotation is given by

$$R(\phi_n) = \begin{bmatrix} cos^2\phi_n & sin^2\phi_n & 0 & 0 & 0 & sin2\phi_n \\ sin^2\phi_n & cos^2\phi_n & 0 & 0 & 0 & -sin2\phi_n \\ 0 & 0 & 1 & 0 & 0 & 0 \\ 0 & 0 & 0 & cos\phi_n & -sin\phi_n & 0 \\ 0 & 0 & 0 & sin\phi_n & cos\phi_n & 0 \\ -\frac{1}{2}sin2\phi_n & \frac{1}{2}sin2\phi_n & 0 & 0 & 0 & cos2\phi_n \end{bmatrix} \tag{E.3}$$

Hence, the density-normalized stiffness matrix of the effective medium is

$$C_e = C_b[I + \{R(\phi_1)\Delta_1 R^T(\phi_1) + R(\phi_2)\Delta_2 R^T(\phi_2)\}C_b]^{-1} \tag{E.4}$$

So, the stiffness coefficient matrix for the monoclinic media with a horizontal symmetry plane is:

$$C_{mono} = \begin{bmatrix} c_{11} & c_{12} & c_{13} & 0 & 0 & c_{16} \\ & c_{22} & c_{23} & 0 & 0 & c_{26} \\ & & c_{33} & 0 & 0 & c_{36} \\ & & & c_{44} & c_{45} & 0 \\ & & & & c_{55} & 0 \\ & & & & & c_{66} \end{bmatrix} \tag{E.5}$$

where c_{ij} with i,j = 1,..,6 are elements of the matrix.

F: Gradient term in the reflection coefficient of AVAz attribute for different wave modes

MODEL A - VTI OVER VFTI

For the model with VFTI media as the lower layer, reflection coefficient for PP wave mode is given as

$R_{PP}(\theta,\phi) = -\frac{\Delta\delta_N(-2+\zeta^2)^2}{4\zeta^4} + \frac{(4\Delta\delta_V\zeta^2 cos^2\phi + \Delta\delta_N(2-\zeta^2)(\zeta^2+2cos2\phi))}{4\zeta^4} sin^2\theta_P$

where, $\zeta = \frac{\overline{V_P}}{\overline{V_S}} = 1.82$ for the model.

The gradient terms using standard VTI model (Schoenberg and Helbig, 1997) are,

$$G_{PP}(\phi) = \frac{-(\zeta^4-4)\delta_N + 4\zeta^2\delta_V}{4\zeta^4} cos^2\phi - \frac{(\zeta^2-2)^2\delta_N}{4\zeta^4} sin^2\phi \tag{F.1}$$

$$G_{S_V-S_V}(\phi) = 0.70\delta_N + 0.50\delta_V - 0.70\delta_N sin^4(\phi) + (-0.25\delta_N + 0.25\delta_H) sin^2 2\phi - (0.40\delta_N + \delta_V) cos^2\phi \tag{F.2}$$

$$G_{S_H-S_H}(\phi) = 0.25\delta_H + (0.08\delta_N - 0.4\delta_H) sin^2 2\phi \tag{F.3}$$

$$G_{P-S_V}(\phi) = \frac{\delta_V\zeta^3 + \delta_N(2-\zeta^2)}{\zeta^{7/2}(1+\zeta)} cos^2\phi \tag{F.4}$$

$$G_{P-S_H}(\phi) = -\frac{\delta_V\zeta^3 + \delta_N(2-\zeta^2)}{\zeta^{7/2}(1+\zeta)} cos\phi sin\phi \tag{F.5}$$

$$G_{S_V-S_H}(\phi) = 0 \tag{F.6}$$

MODEL B - VTI OVER MONOCLINIC

For the model with monoclinic media as the lower layer, the gradient terms are given as,

$$G_{PP}(\phi) = \frac{\Delta c_{33}}{4\overline{c_{33}}} - \left[\frac{\Delta c_{13} cos^2\phi + \Delta c_{23} sin^2\phi + \Delta c_{36} sin2\phi}{2\overline{c_{33}}}\right] + \frac{1}{\zeta^2}\left[\frac{\Delta c_{55} cos^2\phi + \Delta c_{44} sin^2\phi + \Delta c_{45} sin2\phi}{\overline{c_{33}}}\right] \tag{F.7}$$

$$G_{S_V-S_V}(\phi) = -\frac{\Delta c_{33}}{4\overline{c_{33}}} - \left[\frac{\Delta c_{11} cos^4\phi + \Delta c_{22} sin^4\phi}{4\overline{c_{33}}}\right] + \left[\frac{\Delta c_{13} cos^2\phi + \Delta c_{23} sin^2\phi}{2\overline{c_{33}}}\right] - \left[\frac{\Delta c_{12} + 2\Delta c_{66} sin^2\phi}{8\overline{c_{33}}}\right] sin^2 2\phi + \frac{\Delta c_{36}}{\overline{c_{33}}} cos\phi sin\phi - \frac{\Delta c_{16}}{\overline{c_{33}}} cos^3\phi sin\phi - \frac{\Delta c_{26}}{\overline{c_{33}}} cos\phi sin^3\phi \tag{F.8}$$

$$G_{S_H-S_H}(\phi) = \frac{1}{\zeta^2}\left[\frac{\Delta c_{16}-\Delta c_{26}}{8\overline{c_{55}}}sin4\phi - \frac{\Delta c_{66}}{4\overline{c_{55}}}cos^2 2\phi - \frac{\Delta c_{11}+\Delta c_{22}-2\Delta c_{12}}{16\overline{c_{55}}}sin^2 2\phi\right] \tag{F.9}$$

$$G_{P-S_V}(\phi) = \frac{\sqrt{\zeta}}{1+\zeta}\left[-\frac{\Delta c_{13}cos^2\phi + \Delta c_{23}sin^2\phi + \Delta c_{36}sin2\phi}{2\overline{c_{33}}} + \frac{1}{\zeta}\frac{(\Delta c_{55}cos^2\phi + \Delta c_{44}sin^2\phi + \Delta c_{45}sin2\phi)}{\overline{c_{55}}}\right] \tag{F.10}$$

$$G_{P-S_H}(\phi) = \frac{\sqrt{\zeta}}{1+\zeta}\left[\frac{(\Delta c_{13}-\Delta c_{23})sin2\phi - 2\Delta c_{36}cos2\phi}{4\overline{c_{33}}} + \frac{1}{\zeta}\frac{(\Delta c_{44}-\Delta c_{45})sin2\phi + 2\Delta c_{45}cos2\phi)}{2\overline{c_{55}}}\right] \tag{F.11}$$

$$G_{S_V-S_H}(\phi) = 0 \tag{F.12}$$

G: MATLAB codes for plotting well log data and Backus averaging

WELL LOG DATA PLOT

```
close all
fid = xlsread('C:\Petroleum geosc\Specialization\students\Log.xlsx');
depth = fid(:,1); % Depth
rho=fid(:,2);       % Density
vp=fid(:,3);          % P-wave velocity
vs=fid(:,4);          % S-wave velocity
epsilon=fid(:,5);     % Thomsen anisotropic parameters
deltA=fid(:,6);
gamma=fid(:,7);
rho(rho < 1.0) = 0; % to remove any abnormal values
rho(rho > 8) = 0;
for i=1:length(vp)
  c33=rho.*vp.^2/10^6;
  c44=rho.*vs.^2/10^6;
end
  figure(1)
 subplot(1,8,1)
   max_depth=2220;
h = plot(rho,depth,'r','LineWidth',1);
set(gca,'ydir','reverse');
set(gca,'fontweight','bold','fontsize',10);
 axis([1.5 3  0 max_depth]);
 xlabel('Density(g/cc)','fontsize',12);
 ylabel('Depth(m)','fontsize',12);
 grid on
  subplot(1,8,2)
 max_depth=2220;
h = plot(vp,depth,'g','LineWidth',1);
```

```
 set(gca,'ydir','reverse');
 set(gca,'fontweight','bold','fontsize',10);
  axis([1000 5000  0 max_depth]);
  xlabel('Vp (m/s)','fontsize',12);
 grid
 subplot(1,8,3)
  max_depth=2220;
 h = plot(vs,depth,'c','LineWidth',1);
 set(gca,'ydir','reverse');
 set(gca,'fontweight','bold','fontsize',10);
  axis([800 3000  0 max_depth]);
  xlabel('Vs (m/s)','fontsize',12);
 grid

subplot(1,8,4)
  max_depth=2220;
 h = plot(epsilon,depth,'y','LineWidth',1);
 set(gca,'ydir','reverse');
 set(gca,'fontweight','bold','fontsize',10);
  axis([-0.2 0.4  0 max_depth]);
  xlabel('\epsilon','fontsize',12);
 grid
subplot(1,8,5)
  max_depth=2220;
 h = plot(deltA,depth,'m','LineWidth',1);
 set(gca,'ydir','reverse');
 set(gca,'fontweight','bold','fontsize',10);
  axis([-0.2 0.4  0 max_depth]);
  xlabel('deltA','fontsize',12);
 grid

subplot(1,8,6)
  max_depth=2220;
 h = plot(gamma,depth,'k','LineWidth',1);
 set(gca,'ydir','reverse');
 set(gca,'fontweight','bold','fontsize',10);
  axis([-0.2 0.4  0 max_depth]);
  xlabel('\gamma ','fontsize',12);
 grid

 subplot(1,8,7)
  max_depth=2220;
 h = plot(c33,depth,'b','LineWidth',1);
 set(gca,'ydir','reverse');
 set(gca,'fontweight','bold','fontsize',10);
   axis([0 40  0 max_depth]);
  xlabel('C_{33}(GPa) ','fontsize',12);
 grid
 subplot(1,8,8)
  max_depth=2220;
 h = plot(c44,depth,'b','LineWidth',1);
 set(gca,'ydir','reverse');
 set(gca,'fontweight','bold','fontsize',10);
```

```
    axis([0 20  0 max_depth]);
   xlabel('C_{44}(GPa) ','fontsize',12);
  grid
```

BACKUS AVERAGE- EFFECTIVE BACKGROUND MEDIUM PARAMETERS

```
close all
fid = xlsread('C:\Petroleum geosc\Specialization\students\Log.xlsx');
depth = fid(:,1);
 rho=fid(:,2);
 vp=fid(:,3);
 vs=fid(:,4);
 epsilon=fid(:,5);
 deltA=fid(:,6);
 gamma=fid(:,7);
 % Stiffness coeficients from anisotropic parameters and wave velocities
 for i=1:length(vp)
   C33(i)=rho(i).*vp(i).^2/10^6;
   C44(i) =rho(i).*vs(i).^2/10^6;
   C11(i)=C33(i)*(1+(2*epsilon(i)));
   C13(i)=sqrt((C33(i)-C44(i))*(C33(i)*(1+2*deltA(i))-C44(i)))-C44(i);
   C66(i)=C44(i)*(1+(2*gamma(i)));
   C12(i)=(C11(i)-(2*C66(i)));
 end
 % BACKGROUND MODEL 1
 N = 112; % No. of measurement points
 a3 = 1/C33(7424);
     a4 = 1/C44(7424);
     a13 = C13(7424)/C33(7424);
     a11 = C11(7424) -C13(7424)*C13(7424)/C33(7424);
     a66 = C66(7424);
     ad = rho(7424);
for j= 1: N-1    %  Zone for the model 1

    A3(j)=  a3 + 1/C33(7424+j);
     A4(j)=  a4 + 1/C44(7424+j);
     A13(j) =  a13 + C13(7424+j)/C33(7424+j);
     A11(j)= a11 + C11(7424+j)- C13(7424+j)*C13(7424+j)/C33(7424+j);
      A66(j)= a66 + C66(7424+j);
      density1(j) = ad + rho(7424 +j);
     a3 = A3(j);
     a4 = A4(j);
     a13 =  A13(j);
     a11 = A11(j);
     a66 = A66(j);
     ad = density1(j);
end
    C33b1= N/A3(N-1);  % Backus averaged Effective Cij for VTI background
    C44b1 = N/A4(N-1);
    C13b1 = A13(N-1)/A3(N-1);
    C11b1 = A11(N-1)/N + A13(N-1)* A13(N-1)/A3(N-1)/N;
    C66b1 = A66(N-1)/N;
```

```
    C12b1 = C11b1 - 2*C66b1;
    RHOb1 = density1(N-1)/N;
    % Vp, Vs, Effective Thomsen anisotropic parameters for VTI background
    Vpb1 =sqrt(C33b1/ RHOb1);
    Vsb1 =sqrt(C44b1/ RHOb1);
   epsb1=(C11b1-C33b1)/(2*C33b1);
   deltAb1=((C13b1+C44b1)^2-(C33b1-C44b1)^2)/(2*C33b1*(C33b1-C44b1));
   gammab1=(C66b1-C44b1)/(2*C44b1);

 % BACKGROUND MODEL 2
  N = 112; % No. of measurement points
 b3 = 1/C33(10757);
     b4 = 1/C44(10757);
     b13 = C13(10757)/C33(10757);
     b11 = C11(10757) -C13(10757)*C13(10757)/C33(10757);
     b66 = C66(10757);
      bd = rho(10757);
for j= 1: N-1    %  Zone for the model 2

    B3(j)=  b3 + 1/C33(10757+j);
     B4(j)=  b4 + 1/C44(10757+j);
     B13(j) =  b13 + C13(10757+j)/C33(10757+j);
     B11(j)= b11 + C11(10757+j)- C13(10757+j)*C13(10757+j)/C33(10757+j);
      B66(j)= b66 + C66(10757+j);
      density2(j) = bd + rho(10757 +j);
     b3 = B3(j);
     b4 = B4(j);
     b13 =  B13(j);
     b11 = B11(j);
     b66 = B66(j);
     bd = density2(j);
end
    C33b2= N/B3(N-1);  % Backus averaged Effective Cij for VTI background
    C44b2 = N/B4(N-1);
    C13b2 = B13(N-1)/B3(N-1);
    C11b2 = B11(N-1)/N + B13(N-1)* B13(N-1)/B3(N-1)/N;
    C66b2 = B66(N-1)/N;
    C12b2 = C11b2 - 2*C66b2;
     RHOb2 = density2(N-1)/N;
    % Vp, Vs, Effective Thomsen anisotropic parameters for VTI background
    Vpb2 =sqrt(C33b2/ RHOb2);
    Vsb2 =sqrt(C44b2/ RHOb2);
   epsb2=(C11b2-C33b2)/(2*C33b2);
   deltAb2=((C13b2+C44b2)^2-(C33b2-C44b2)^2)/(2*C33b2*(C33b2-C44b2));
   gammab2=(C66b2-C44b2)/(2*C44b2);
```

H: Error in orientation of fracture sets determined by inverse modeling for Monoclinic model 1 and 2 derived from well log data

Case 1: when the fracture weaknesses of both fracture sets are identical,
$\delta_{N1} = \delta_{N2} = 0.1$
$\delta_{V1} = \delta_{V2} = 0.2$
$\delta_{H1} = \delta_{H2} = 0.3$

Case 2: when the fracture weaknesses of fracture sets are non-identical,

In this case,
$\delta_{N1} = 0.1, \delta_{N2} = 0.15$
$\delta_{V1} = 0.2, \delta_{V2} = 0.2$
$\delta_{H1} = 0.3, \delta_{H2} = 0.35$

Fracture weaknesses	Identical for both fracture sets			Different for fracture sets	
Actual azimuth angles (fracture orientation)	Wave modes considered	Error (°)		Error (°)	
		$\Delta\phi_1$	$\Delta\phi_2$	$\Delta\phi_1$	$\Delta\phi_2$
$\phi_1 = 20°$, $\phi_2 = -15°$	P,S_1	-0.03	-0.01	-0.02	-0.01
	P,S_2	-0.03	-0.01	-0.02	-0.01
	S_1,S_2	-0.03	-0.001	0.01	-0.001
$\phi_1 = 30°$, $\phi_2 = -20°$	P,S_1	0.12	0.11	0.11	-0.1
	P,S_2	-0.01	0.03	0.05	-0.02
	S_1, S_2	-0.31	0.03	-0.03	0.02
$\phi_1 = 45°$, $\phi_2 = -30°$	P,S_1	0.15	0.15	2.5	-0.11
	P,S_2	-0.62	0.02	-0.03	0.02
	S_1, S_2	-0.35	-0.5	-2.5	0.75
$\phi_1 = 60°$, $\phi_2 = -45°$	P,S_1	1.52	0.53	1.55	2.45
	P,S_2	1.53	0.5	-45.5	7.65
	S_1, S_2	3.45	0.5	-35.5	6.45
$\phi_1 = 60°$, $\phi_2 = -60°$	P,S_1	Non-	Non-	1.5	-1.78
	P,S_2	Unique	Unique	1.1	-1.5
	S_1, S_2	solutions	solutions	62.35	–67.59

Table 7: Error in estimation of azimuth angles using Group velocity coefficient A_{11} for Model 1.

Fracture weaknesses	Identical for both fracture sets			Different for fracture sets	
Actual azimuth angles (fracture orientation)	Wave modes considered	Error (°)		Error (°)	
		$\Delta\phi_1$	$\Delta\phi_2$	$\Delta\phi_1$	$\Delta\phi_2$
$\phi_1 = 20°$, $\phi_2 = -15°$	P,S_1	-0.11	0.13	-0.1	0.11
	P,S_2	-0.16	0.11	-0.12	0.10
	S_1, S_2	0.02	0.01	0.01	0.005
$\phi_1 = 30°$, $\phi_2 = -20°$	P,S_1	0.6	1.4	0.43	1.11
	P,S_2	0.51	1.41	0.45	1.12
	S_1, S_2	0.004	0.03	0.002	0.02
$\phi_1 = 45°$, $\phi_2 = -30°$	P,S_1	-4.5	-3.6	-2.5	-2.13
	P,S_2	-3.11	-1.43	-1.31	0.5
	S_1, S_2	0.515	-0.52	-1.35	0.45
$\phi_1 = 60°$, $\phi_2 = -45°$	P,S_1	-1.8	1.5	1.35	3.15
	P,S_2	1.23	-0.85	-5.65	6.35
	S_1, S_2	2.25	-0.55	-4.75	5.85
$\phi_1 = 60°$, $\phi_2 = -60°$	P,S_1	Non-	Non-	1.41	-1.32
	P,S_2	Unique	Unique	1.12	-0.95
	S_1, S_2	solutions	solutions	3.78	-3.50

Table 8: Error in estimation of azimuth angles using Group velocity coefficient A_{11} for Model 2.

I: NMO ellipses sensitivities to Thomsen parameters

Stiffness coefficients of the VTI media can be written in terms of c_{33}, c_{44} and Thomsen parameters ϵ, γ and δ. (Thomsen, 1986)
$c_{11} = c_{33}(1 + 2\epsilon)$
$c_{66} = c_{44}(1 + 2\gamma)$
$c_{12} = c_{33}(1 + 2\epsilon) - 2c_{44}(1 + 2\gamma)$
$c_{13} = \sqrt{2c_{33}(c_{33} - c_{44})\delta + (c_{33} - c_{44})^2} - c_{44}$
$c_{33} > c_{44} > 0$

VFTI MEDIA

Coefficients infront of fracture weaknesses in the equations for squared NMO velocities for different wave modes can be related with Thomsen parameters of background media. This means that the coefficients can be linearized as

$$A(\delta_f) = b_0 + b_\epsilon\epsilon + b_\gamma\gamma + b_\delta\delta \tag{I.1}$$

Where, δ_f is the fracture weakness
b_0 = isotropic coefficient
$b_\epsilon, b_\gamma, b_\delta$ are respective coefficients of the Thomsen parameters ϵ, γ, δ of background VTI media. Using the data from standard model for the VTI background (Schoenberg Helbig, 1997), such equations are obtained for pure (PP) and converted (PS_1) wave modes in XZ and YZ symmetry planes denoted by subscripts 1 and 2 respectively.

For PP wave mode:
$A(\delta_N)_1 = -3.3 - 1.3\epsilon - 12\delta$
$A(\delta_N)_2 = -0.6 - 6.6\epsilon + 5.3\gamma$
$A(\delta_V)_1 = -8 - 12\delta$
$A(\delta_V)_2 = 0$
$A(\delta_H)_1 = 0$
$A(\delta_H)_2 = 0$

For PS_1 wave mode:
$A(\delta_N)_1 = -3.3 - 5.6\epsilon + 1.5\delta$
$A(\delta_N)_2 = -0.19 - 1.9\epsilon + 1.34\gamma + 0.19\delta$
$A(\delta_V)_1 = 2.9 - 22.5\epsilon + 37\delta$
$A(\delta_V)_2 = 0$
$A(\delta_H)_1 = 0$
$A(\delta_H)_2 = -1.73 - 1.73\gamma - 1.73\delta$

MONOCLINIC MEDIA

Group velocity coefficient responsible for rotation of NMO group ellipses (A_{11}) for different wave modes is considered. This coefficient is analyzed for sensitivities to Thomsen parameters of VTI background models derived from well log data. Two different orien-

tations are considered. Azimuth angles of fracture normals for set 1 and set 2 are ϕ_1 and ϕ_2 respectively.

a) $\phi_1 = 30^\circ$ and $\phi_2 = -20^\circ$
Model 1
$A_{11}(P) = 10^{-4}(-2.4 + 4.8\epsilon - 4.8\gamma + 0.4\delta)$
$A_{11}(S_1) = -0.03 + 0.2\epsilon + 0.002\gamma - 0.2\delta$
$A_{11}(S_2) = 0.03 - 0.2\epsilon + 0.001\gamma + 0.2\delta$
Model 2
$A_{11}(P) = 10^{-4}(-2.2 + 4.4\epsilon - 4.4\gamma + 0.02\delta)$
$A_{11}(S_1) = -0.03 + 0.17\epsilon + 0.002\gamma - 0.17\delta$
$A_{11}(S_2) = 0.025 - 0.17\epsilon + 0.001\gamma + 0.17\delta$

b) $\phi_1 = 45^\circ$ and $\phi_2 = -30^\circ$
Model 1
$A_{11}(P) = 10^{-4}(-1.4 + 2.9\epsilon - 2.9\gamma + 0.26\delta)$
$A_{11}(S_1) = -0.04 + 0.25\epsilon + 0.005\gamma - 0.25\delta$
$A_{11}(S_2) = 0.04 - 0.25\epsilon - 0.0026\gamma + 0.25\delta$
Model 2
$A_{11}(P) = 10^{-4}(-1.3 + 2.6\epsilon - 2.6\gamma + 0.01\delta)$
$A_{11}(S_1) = -0.03 + 0.22\epsilon + 0.005\gamma - 0.22\delta$
$A_{11}(S_2) = 0.03 - 0.22\epsilon - 0.0025\gamma + 0.22\delta$

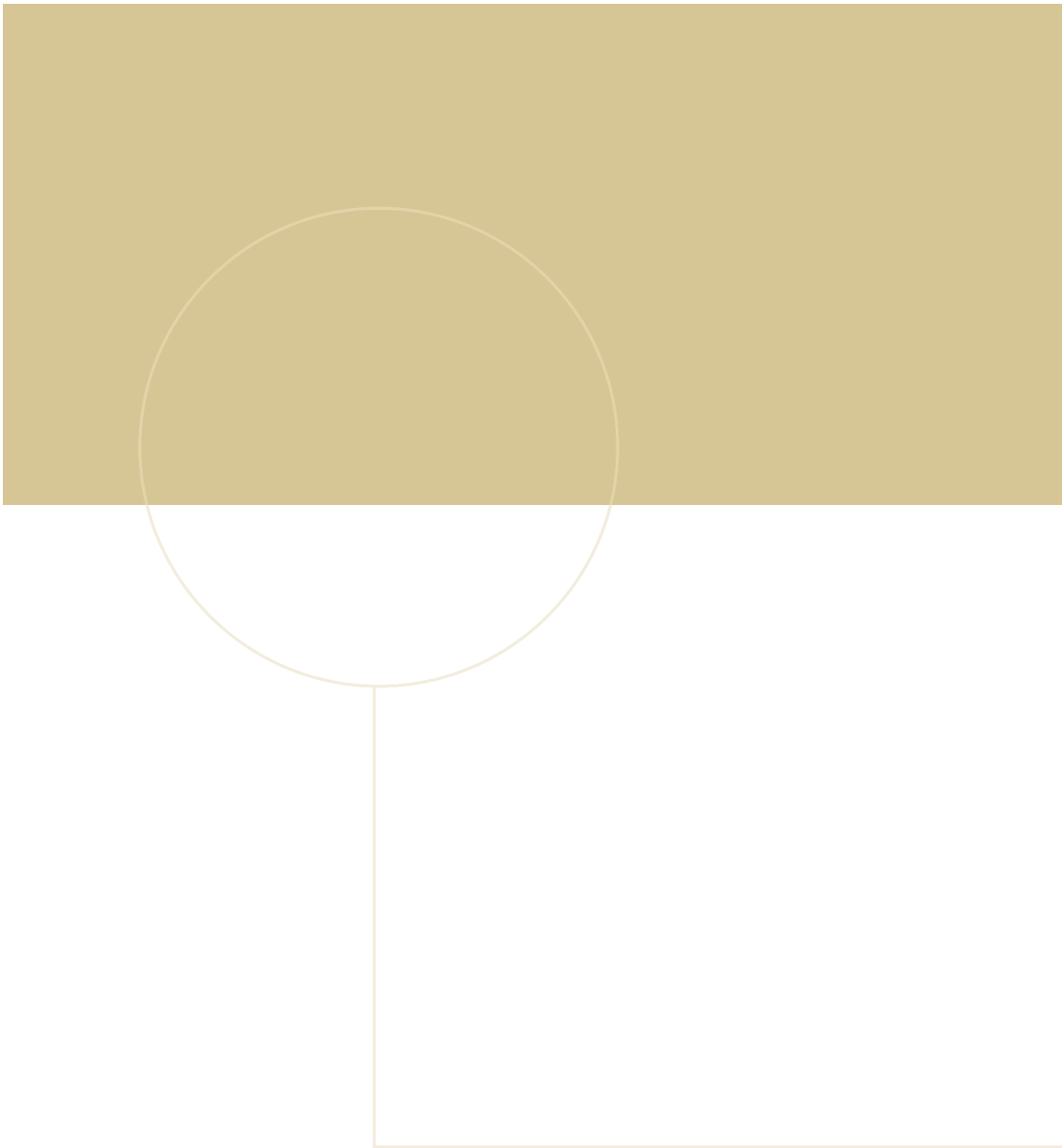

NTNU

Norwegian University of
Science and Technology